Slow deactivation of RuBisCO elucidated by mathematical models

Franziska Witzel[1,2]
franziska.witzel@charite.de

Jan Götze[3]
jgoetze@uni-potsdam.de

Oliver Ebenhöh[2,4]
ebenhoeh@abdn.ac.uk

[1] Max-Planck-Institute for Molecular Plant Physiology, Potsdam-Golm, Germany
[2] Institute for Pathology, Charité, Berlin, Germany
[3] Institute for Chemistry, University of Potsdam, Germany
[4] Institute for Complex Systems and Mathematical Biology, University of Aberdeen, United Kingdom
[5] Institute of Medical Sciences, University of Aberdeen, United Kingdom

Corresponding author: Oliver Ebenhöh, University of Aberdeen, Institute for Complex Systems and Mathematical Biology, Aberdeen, AB24 3UE, United Kingdom
Email: ebenhoeh@abdn.ac.uk, Tel. +44 (0)1224 272520

Running title: Modeling the slow deactivation of RuBisCO

Abbreviations:

RuBisCO	ribulose-1,5-bisphosphate oxygenase/carboxylase
RuBP	ribulose-1,5-bisphosphate
XuBP	xylulose-1,5-bisphosphate
PDBP	D-*glycero*-2,3-pentodiulose-1,5-bisphosphate
PGA	3-phosphoglyceric acid
PG	2-phosphoglycolate
DP1P	deoxypentodiulose phosphate

Key words: Rubisco, photosynthesis, carbon fixation, fallover, mathematical model, enzyme kinetics

Abstract

Ribulose-1,5-bisphosphate carboxylase/oxygenase (RuBisCO) is the key enzyme of the Calvin cycle, catalyzing the fixation of inorganic carbon dioxide to organic sugars. Unlike most enzymes, RuBisCO is extremely slow, substrate unspecific, and catalyzes undesired side-reactions which are held responsible for the slow deactivation observed *in vitro*, a phenomenon known as fallover. Despite the fact that amino acid sequences and 3D structures of RuBisCO from a variety of species are known, the precise molecular mechanisms for the various side reactions are still unclear. Here, we investigate the kinetic properties of RuBisCO using mathematical models. Initially, we formulate a minimal model that quantitatively reflects the kinetic behavior of RuBisCOs from different organisms. By relating rate parameters for single molecular steps to experimentally determined K_M and $V_{\max}$ values, we can examine mechanistic differences among species. The minimal model further demonstrates that two inhibitor producing side reactions are sufficient to describe experimentally determined fallover kinetics. To explain the observed kinetics of RuBisCO's limited capacity to accept xylulose-1,5-bisphosphate as substrate, inclusion of other side reactions is necessary. Our model results suggest a yet undescribed alternative enolization mechanism that is supported by the molecular structure. Taken together, the presented models serve as a theoretical framework to explain a wide range of observed kinetic properties of RuBisCOs derived from a variety of species. We can thus support hypotheses about molecular mechanisms and systematically compare enzymes from different origins.

Introduction

The enzyme ribulose-1,5-bisphosphate carboxylase/oxygenase (RuBisCO, EC 4.1.1.39), responsible for the major part of the global flux from inorganic to organic carbon, is in many respects unlike other enzymes. Its overall catalytic rate is extremely small (only around 3 s^{-1} in higher plants). This slowness in conjunction with its central importance for the carbon metabolism of any photosynthetic organism, and thus for the biosphere as a whole, explains its extremely high abundance. Estimations are that RuBisCO accounts for 50% of the total soluble protein in a plant cell [1]. In the chloroplast stroma of plant leaves, a typical concentration of RuBisCO is 0.4 mM which corresponds to approximately 240 mg/ml [2]. RuBisCO is also special with respect to its structure and structural variations found among photosynthetic organisms. Different RuBisCOs are commonly devided into four types (types I-IV), where type I is subdivided into 4 distinct classes (A-D) based on sequence homology [3]. In all investigated higher plants, RuBisCO of type IB is found, which is present as a hexadecamer consisting of eight large, plastid encoded, and eight small, nuclear encoded, subunits, a configuration compactly denoted as L8S8, with a total molecular mass of approximately 550 kDa [4]. In some photosynthetic prokaryotes (purple non-sulfur bacteria, several chemoautotrophic bacteria) and the eukaryotic dinoflagellates, a simpler form of RuBisCO is found, present as a dimer of two large subunits (L2) [5]. Apparently, this is also the minimal configuration with catalytic activity since, despite the differences in structural details, all forms of RuBisCO share the common property that the catalytic centers are located at the interface of two large subunits [6]. The sequence identity of the large subunits throughout forms I-IV of about 25-30 % leads to a highly conserved 3D-structure [5].

RuBisCO displays some unexpected catalytic properties. In contrast to most enzymes, it is not substrate specific but also catalyzes oxygenation by accepting molecular oxygen as second substrate, resulting in the release of one molecule 3-phosphoglyceric acid (PGA) and one molecule 2-phosphoglycolate (PG). The latter has to be recycled in a complex pathway involving several cellular compartments, ATP consumption and the loss of carbon dioxide. The oxygenation therefore results in a lower net efficiency of the carbon fixation process and it seems plausible that evolution has favored RuBisCOs minimizing this photorespiration. A second unusual phenomenon, found exclusively in the L8S8 configuration in higher plants, is the slow loss of catalytic activity of isolated RuBisCO *in vitro*. This process is vividly termed fallover [7, 8, 9, 10, 11, 12] and is accounted to the formation of tightly binding inhibitors at the active site. Because of the ATP dependent constant removal of inhibitors from the active site by the enzyme rubisco activase [13, 14], this effect is not observed *in vivo*. The extent to which activity is reduced during fallover as well as the characteristic time in which this process takes place is highly dependent on the external conditions, in particular ambient CO_2 and O_2 concentrations. These quantities also seem to vary significantly among species and small mutations such as single amino-acid exchanges, as demonstrated by Pearce and Andrews [15], may have a drastic effect.

The enzyme kinetics of RuBisCO has been subject to theoretical investigations at the level of kinetic modelling and quantum chemical calculations [16, 17, 18, 19, 20, 21]. Commonly, when *in vitro* experiments are interpreted, various inhibition processes contributing to fallover are fitted to a simple exponential curve [7, 10, 11, 12, 15], resulting in the estimation of characteristic times and apparent inhibition constants. While this approach is adequate for obtaining heuristic parameters from experimental data, it does not provide a mechanistic understanding of the underlying principles. McNevin and coworkers [20] have developed a detailed kinetic model of RuBisCO that includes the reversible steps of activation which are the addition of an activator CO_2 molecule and the subsequent binding of the central Mg^{2+} ion that stabilizes the carbamate and completes the active site. Their model also accounts for the competitive binding of the substrate ribulose-1,5-bisphosphate (RuBP) and the inhibitor xylulose-1,5-bisphosphate (XuBP) as well as the formation of the latter at the active site. The main purpose of their analysis was to estimate the rates of the elementary chemical steps. For this, 18 parameters were simultaneously fitted to experimental time curves. The large number of parameters implies a high uncertainty in the prediction. In fact, the estimated release rate of XuBP, for example, is orders of magnitude larger than experimentally observed production rates [11].

In this paper, we present a minimal mathematical model that was formulated based on mechanistic considerations and derived by the motivation to explain the dynamics of the fallover effect. Due to its simplicity the model provides a theoretical framework to explain the underlying principles of the fallover phenomenon and other peculiar dynamic properties of RuBisCO. In our model, we only consider fully activated enzyme, because firstly *in vitro* studies on the fallover effect are conducted with fully activated RuBisCO [7, 8, 9, 10, 11, 15, 22], and secondly decarbamylation is slow [23] and only occurs at low Mg^{2+} concentrations [10] or low pH values [24]. We demonstrate that including the binding steps of the activator CO_2 and Mg^{2+} is not necessary to explain the fallover effect. We do, however, include the biologically very relevant oxygenation pathway, which is inevitably active under *in vivo* and oxygenic *in vitro* conditions.

In its simplest form, our model is capable of explaining which intrinsic parameters are

important for the fallover extent and characteristic times. Simple relations between rate parameters and experimentally accessible quantities are derived, allowing for an easy fit of parameters to various types of RuBisCO. This allows to identify key features determining the distinct kinetic behaviors of different RuBisCOs.

However, the basic model is unable to explain other important characteristics, in particular the two types of inhibition (rapid equilibrium and slow) exhibited by XuBP [25]. We show how the model has to be extended to also explain this behaviour and arrive at a hypothesis of an intermediate state which has not yet been described. Introduction of this intermediate into the model is necessary to explain the slow loss of catalytic activity that also occurs when XuBP is applied as a substrate [15] .

Results

Model Formulation

We develop a minimal model containing the main carboxylating and oxygenating activities and the two side reactions resulting in the formation of two tight binding inhibitors which were found to be the major causes for the fallover effect [11]. The model is schematically represented in Fig. 1, in which the main reactions are contained in the highlighted box and marked by bold arrows. Substrate binding to the free carbamylated enzyme E and abstraction of a proton from the C3 carbon of RuBP [18], in which a 2,3-enediol is formed, are described as a single step, proceeding with rate v_{ER}. The enediol intermediate ER may bind either CO_2 (rate v_{ERC}) or O_2 (v_{ERO}) as second substrate. In both cases, cleavage and product release are again described as a single step (v_{cat} and v_{oxy}, respectively). These product forming steps have been previously covered in computational models [19, 21] and are generally assumed to proceed in a strict consecutive order. The inhibitor XuBP may result from the enediol intermediate ER by reversing enolization but with a proton being attached from the 'wrong' side (v_{EI1}). After oxygenation of the enediol intermediate, the resulting peroxyketone ERO may undergo a loss of hydrogen peroxide (v_{EI2}), yielding D-*glycero*-2,3-pentodiulose-1,5-bisphosphate (PDBP). In some RuBisCOs, this may be further rearranged to form 2'-carboxytetritol-1,5-bisphosphate [11, 26], but this step is not reflected in our model.

All elementary reaction rates are assumed to follow mass action kinetics (a full set of equations is given in the Supplementary Text S1). The last catalytic steps of the carboxylation or oxygenation are assumed to be irreversible, because under *in-vivo* as well as *in-vitro* conditions, the products are rapidly processed by other enzymes. Unless otherwise stated, we assume that the concentrations of substrates remain constant. This is realistic for most *in-vitro* studies in which typical enzyme concentrations are orders of magnitude lower than substrate levels.

RuBisCO is assumed to remain carbamylated throughout fallover, as has been experimentally demonstrated in [8]. Thus, all enzyme species contained in the model refer to fully activated RuBisCO. We further presume that all eight active sites of RuBisCO work independently of each other [27] which has been proven experimentally at least for the affinity of RuBisCO for its first substrate RuBP [28].

The observed time scale of fallover lies in the range of minutes and is thus orders of magnitude slower than the overall carboxylation and oxygenation reactions. This time

scale separation allows to approximate the intermediate enzyme-substrate complexes ER, ERC, and ERO with a quasi steady state assumption, thereby uncoupling the equations describing fast and slow reactions, respectively. In the following, the fast reactions of the main catalytic pathways and the slow reactions responsible for the fallover phenomenon are studied independently.

Carboxylation and Oxygenation

In many experiments, in particular those in which kinetic constants such as K_M-values are determined, the initial turnover rate of activated RuBisCO is measured directly after application of the substrate. This initial rate corresponds to a quasi steady state that the system rapidly assumes before any relevant amounts of inhibitors have been formed. The initial quasi steady state expressions (for a derivation, see Supplementary Text S2) allow to relate kinetic parameters of the main pathways to measurable quantities, in particular the $V_{\max}$ and K_M values and the C/O-specificity Ω. With the resulting formulas 11–17 (see Methods), experimental data can be optimally exploited to calculate the rate parameters for catalysis of carboxylation (k_{cat}) and oxygenation (k_{oxy}), as well as the binding rate parameter for the first substrate RuBP (k_{ER}^{+}). We also obtain the two derived parameters

$$\gamma = \frac{k_{ERC}^{+}}{k_{ERC}^{-} + k_{cat}} \qquad \text{and} \qquad \omega = \frac{k_{ERO}^{+}}{k_{ERO}^{-} + k_{EI2}^{+} + k_{oxy}} \tag{1}$$

which are closely related to the binding processes of the second substrates CO_2 and O_2, respectively.

In contrast to an approach in which all parameters are simultaneously fitted, the danger of overfitting is excluded, because it becomes immediately apparent which parameters cannot contribute to an improved fit and thus have to be estimated or derived from other sources of information. Moreover, the analytic expressions allow to infer directly which parameters or parameter combinations are most influential on the observed quantities. The resulting sensitivities are summarized in Fig. 2, where red fields denote a positive and blue fields a negative influence. All other rate parameters play only an insignificant role for the analyzed quantities. Remarkably, for all investigated organisms, the distribution of these sensitivity values is almost identical. Moreover, only values near 0 or ± 1 are observed. The maximal rate only depends on the catalytic turnover rate. Binding rates negatively influence the respective K_M-values. The carboxylation rate positively influences the K_M-values for RuBP and CO_2 while oxygenation rate exerts a positive effect on the K_M-value for O_2. As expected, C/O-specificity is increased with faster binding of CO_2, while it is decreased for faster O_2 binding rates.

We have retrieved $V_{\max}$, K_M and specificity values for RuBisCOs originating from a wide range of species. Using the experimental errors stated in the original literature [29, 11, 30, 31, 32, 33, 34], we have calculated possible ranges for the kinetic model parameters and summarized the results in Table 1. It can be observed that the oxygenation rate constants of the different types of RuBisCO are rather similar. In contrast, drastic differences are observed in the carboxylation rate constants, the binding rate constants for RuBP and the parameters γ and ω. For example, RuBisCO from *Synechococcus* displays a much larger $V_{\max}$-value than tobacco, and simultaneously the K_M-value for CO_2 is also drastically elevated. As a result, the k_{cat} for *Synechococcus* is roughly four times larger while γ is reduced by a factor of around 30. These results are consistent

with the notion that the substrate CO_2 is bound with a weaker affinity to *Synechococcus* RuBisCO, but the final catalytic step proceeds faster. This again allows the interpretation that in *Synechococcus* the energy level of the intermediate state ERC, in which both substrates are bound to the active center, is significantly elevated as compared to the corresponding intermediate state in tobacco RuBisCO. Inspection of the values for *Galdieria sulfuraria* allows for the opposite interpretation, namely that the intermediate complex ERC possesses a lower energy state in *G. sulfuraria* than in tobacco, explaining the slower catalytic rate and the higher substrate specificity. Among the investigated organisms, *G. sulfuraria* displays the highest K_M-value for RuBP, which results in the lowest model parameter for the binding process of RuBP to the free catalytic center (k_{ER}^+). An equally high C/O-specificity is exhibited by RuBisCO from the red alga *Griffithsia monilis*, which simultaneously displays a similar turnover rate as that of higher plants [35]. It is therefore speculated that incorporating the *G. monilis* enzyme into a C3 plant would potentially double its photosynthetic performance [36].

Among the examined species, only the bacterium *Rhodospirillum rubrum* features the simple L2 configuration, lacking the catalytically inactive small subunit. It exhibits the smallest K_M-value for RuBP, explaining the high value of the rate parameter k_{ER}^+. Again, a possible explanation could lie in different energetic levels of the corresponding intermediate enzyme-substrate complexes. The findings indicate that in the more complicated L8S8 configuration, binding the large substrate RuBP is more difficult, but binding the small molecule CO_2 may be considerably facilitated, possibly as an effect of the small subunits, thus allowing for a considerably increased C/O-specificity.

Side reactions and fallover

The slow reactions (marked by thin arrows in Fig. 1) are responsible for the formation of inhibitors which occupy the catalytic centers. Since the decline of the overall activity does not lead to complete inactivation, it is evident that reactivation of the catalytic centers occurs. This may in principle be achieved by a slow back conversion or a slow inhibitor release or a combination thereof. For our model, we assume that the inhibitor XuBP is not released from the active site ($k_X^- = 0$), whereas PDBP cannot be transformed back ($k_{EI2}^- = 0$). The first assumption is motivated by the experimental observation that free XuBP is almost not detectable in fallover assays [11]. The irreversibility of the formation of PDBP results from the fact that free H_2O_2 would be necessary in millimolar concentrations for the reverse reaction [37].

The model parameters given in Table 2 realistically reproduce the experimental time courses observed for wild type tobacco [15]. Parameters for the fast reactions were obtained as described above (see Table 1). To infer the slow reaction parameters, the time scale separation of the system was exploited to apply a quasi-steady state assumption and the resulting approximation formulas were used to infer combinations of parameters from the measured extents and characteristic times under aerobic and anaerobic conditions (see Methods and Supplementary Text S2). The remaining free parameters were fitted manually. We use this parameter set as a reference to study how fallover is determined by the single rate parameters and how external conditions influence its strength and characteristic time.

Typical simulated time courses of the fallover dynamics under aerobic and anaerobic conditions are depicted in the insets of Fig. 3. Initial ($v_{cat}^i, t = 0$) and final ($v_{cat}^f, t \to \infty$)

rates, as well as the half time $T_{1/2}$, at which the mean of these two rates is reached, are indicated in the plots. To study which internal parameters exert the strongest influence on the fallover dynamics, we systematically varied every single parameter around its reference value and recorded the resulting change in fallover extent and characteristic time (a full list of the response coefficients is found in Supplementary Table S2). For anaerobic conditions, the effect of the the rates involved in inhibitor formation (k^+_{EI1}) or back-conversion (k^-_{EI1}) is depicted in Fig. 3A. A faster inhibitor formation leads to an enhanced fallover extent while faster back-conversion results in its reduction. In contrast, the increase of either parameter will lead to an increased observed fallover rate (k_{obs}) and therefore to a shorter fallover halftime.

The response of the fallover extent, defined as the relative activity decline from the initial value v^i_{cat} to the final value v^f_{cat}, is directly understandable from the approximation formula (see Methods, Eq. 18, and Supplementary Text S2 for the derivation). For the anaerobic case, this simplifies to

$$f = 1 - \frac{v^f_{cat}}{v^i_{cat}} \approx \frac{\Gamma_1}{1 + \frac{[CO_2]}{K_{M(\mathrm{CO_2})}} + \Gamma_1 + \frac{[CO_2]}{K_{M(\mathrm{CO_2})}} \cdot \frac{K_{M(\mathrm{RuBP})}}{[RuBP]}}. \tag{2}$$

Here, the ratio $\Gamma_1 = k^+_{EI1}/k^-_{EI1}$ plays a dominant role. For $\Gamma_1 = 0$, no fallover is observed ($f = 0$) while for large values ($\Gamma_1 \to \infty$), the final activity will reach zero ($f = 1$). The response of the fallover rate can be understood from the particularly simple theoretical expression for k_{obs} in the anaerobic case,

$$k_{\mathrm{obs}} = a k^+_{EI1} + k^-_{EI1}, \tag{3}$$

which results from the fact that the system reduces to a single linear differential equation (see Supplementary Text S2). Here, a is a combination of various system parameters. From its definition it is evident that $a < 1$, explaining why the effect of inhibitor formation rate is less pronounced than the effect exerted by the back-conversion rate.

Under aerobic conditions, the formation and release of the oxygen dependent inhibitor PDBP is an important effector of the fallover dynamics. The response of fallover extent and rate when perturbing the corresponding rate parameters k_{EI2} and k^-_P are shown in Fig. 3B. Again, the bold lines indicate the response of the fallover extent while the dashed lines denote the response of the observed fallover rate. Similar to the case of the inhibitor XuBP, also here increasing the production rate of the inhibitor leads to an increased fallover extent while increasing the release rate decreases the extent. However, the effect is not as pronounced as for the first inhibitor in the anaerobic case. This behavior is understandable from the approximation formula of the fallover extent under aerobic conditions (Methods, Eq. 18), expressed in the form

$$f \approx \frac{\Gamma_1 + \Gamma_2 \frac{[O_2]}{K_{M(\mathrm{O_2})}}}{1 + \frac{[CO_2]}{K_{M(\mathrm{CO_2})}} + \Gamma_1 + (1 + \Gamma_2)\frac{[O_2]}{K_{M(\mathrm{O_2})}} + \frac{[CO_2]}{K_{M(\mathrm{CO_2})}} \cdot \frac{K_{M(\mathrm{RuBP})}}{[RuBP]} + \frac{1}{\Omega}\frac{K_{M(\mathrm{RuBP})}}{K_{M(\mathrm{CO_2})}}\frac{[O_2]}{[RuBP]}}. \tag{4}$$

Here, increasing the ratio $\Gamma_2 = k^+_{EI2}/k^-_P$ results in an increased fallover extent, while decreasing this ratio will dimish the extent.

With oxygen present, the model predicts a time course of fallover which is a superposition of two exponential processes, where the time constants correspond to the eigenvalues

of the reduced Jacobian matrix (see Supplementary Text S2). From experimental data, such a superposition of two exponential decay processes is often hard to distinguish from a simple exponential decay, especially if the data is noisy and plotted on a linear scale. If fitted to an exponential curve, the resulting observed characteristic fallover time constant k_{obs} lies between the two eigenvalues. The influence on the characteristic time is comparable to the anaerobic case only for small changes of the parameters. For larger changes, the more complex behavior reflects the simultaneous influence of several processes.

The fallover dynamics were experimentally analyzed under different substrate concentrations [38, 20, 7, 10, 15]. It was generally observed that fallover is more pronounced in the presence of oxygen in comparison to anaerobic conditions. On the other hand, an increase of CO_2 leads to fallover alleviation. The latter observation is easily explained with the approximation formula 4 for the fallover extent. The CO_2 concentration enters the equation only in the denominator, therefore its increase will inevitably result in a decreased fallover extent. The formula also predicts that increased concentrations of RuBP will lead to an increased fallover extent. This is understandable considering that higher RuBP levels lead to a higher level of the intermediate state ER, from which the enzyme-inhibitor complex EI1, repsonsible for the fallover extent, is formed. However, because under physiological as well as typical *in-vitro* conditions, RuBP is present in concentrations of around 500 μM, which is several factors larger than typical $\mathrm{K}_{M(\mathrm{RuBP})}$-values (see Table 1), this effect is expected to be minimal. For low RuBP concentrations, the formula predicts a reduced fallover extent. However, sub-saturating levels of RuBP induce decarbamylation of RuBisCO [39] and thus lead to an increased level of inactivation which is not captured by our model.

A simple correlation between fallover extent and oxygen concentration cannot be derived. In fact, the formula allows in principle for a positive or negative effect of the external oxygen concentration on the fallover extent. It can, however, be concluded that the higher the CO_2 concentration the more positive the influence of the oxygen concentration on the fallover extent will be. To confirm our theoretical deliberations, we have systematically investigated the effect of external substrate concentrations on the fallover dynamics. In Fig. 4A, the fallover extent is plotted as a function of the external concentrations of CO_2 and O_2. It can in fact be observed that for low CO_2 concentrations the effect of oxygen is only marginal in absolute terms of f. However, increased oxygen results in a large relative decline of the remaining activity, expressed by $1 - f$. For higher CO_2 concentrations, fallover extent increases dramatically with increasing oxygen level. For illustration, the fallover extent is plotted as a function of a single substrate concentration in Fig. 4B, where in the upper panel the dependency on CO_2 at atmospheric oxygen is given and in the lower panel the dependency on oxygen at the typical experimental condition in which 10 mM $NaHCO_3$ is applied to the buffer solution (corresponding to $\approx$ 125 μM CO_2 at 25°C).

The effect of substrate concentrations on the characteristic time is not easily predictable. Fig. 5A depicts the observed half-time (the time at which the catalytic activity reaches the average of the initial and the final rate) as a function of the external concentrations of CO_2 and O_2. Interestingly, increased CO_2 concentrations lead to a slower fallover while the effect of O_2 is non-monotonic. The model predicts that for concentrations of around 100 μM (corresponding to an atmospheric oxygen level of 8%), the fallover should show the slowest dynamics. The only systematic study of the effect of several different oxygen-levels on the fallover dynamics the authors are aware of are found in [10]

which was conducted with RuBisCO isolated from spinach. There, no effect of oxygen on the fallover extent was observed. This can be explained by the attendant low level of atmospheric CO_2 (350 ppm, corresponding to 11 μM). Zhu et al. [38] found an increased fallover extent of RuBisCO from *Arabidopsis thaliana* when they exchanged the oxygen free environment for a pure oxygenic atmosphere in presence of 10 mM HCO_3^-, thus also confirming our theoretical investigation. The measured half-time decreased monotonously with increasing oxygen concentrations [10]. However, no data was obtained for concentrations between 0 and 250 μM (atmospheric conditions) and therefore this finding does not contradict our model predictions. Further, it is likely that the model parameters will slightly differ between spinach, Arabidopsis and tobacco RuBisCO. Considering that small parameter changes might significantly influence fallover extent and characteristic time (see Fig. 3), it is not unlikely that RuBisCOs from different higher plant species will display a quantitatively different fallover behavior.

The multi-faceted role of xylulose-1,5-bisphosphate leads to new mechanistic interpretations

In fallover assays, the slow formation of XuBP is a major cause for the observed activity decline. Applied externally, XuBP acts as a potent inhibitor. When RuBisCO is exposed to a mixture of RuBP and XuBP in an *in vitro* assay, a fast equilibrium, competitive inhibition is observed [25, 40]. However, if RuBisCO is pre-incubated with XuBP for several minutes before application of the substrate RuBP, the inhibitory effect is considerably increased and strongly dependent on the incubation time [25, 15, 41]. XuBP may also act as a substrate, albeit a poor one, with a catalytic activity according to 0.03% of the rate of RuBP carboxylation [40]. Interestingly, even for this extremely slow carboxylation reaction, the catalytic activity subsides in the time range of minutes in analogy to the fallover phenomenon [15].

The minimal model presented above is not capable to explain these various modes of behavior. We minimally modify our model in two respects. Firstly, we consider binding and enolization as several steps. This is necessary to describe the two modes of inhibition acting on different time scales. Secondly, we include the slow formation of another inhibitor which may also arise from the enediol intermediate, which is required to explain the slow activity decline on XuBP as substrate. The more detailed model is schematically depicted in Fig. 6 and the full set of kinetic equations is given in Supplementary Text S3.

The biphasic inhibitor properties have been experimentally described in detail by McCurry et al. [25]. Their observations suggest that the biphasic inhibitory behavior of XuBP arises from a fast binding step determining the short term behavior observed when applying a mixture of sugars, and a slow conversion to an enediol intermediate which is dominating during incubation. In Fig. 7, the simulated effect of pre-incubating the activated enzyme with XuBP is plotted as a function of incubation time for different inhibitor concentrations (the full set of parameters reflecting wild-type RuBisCO is given in Supplementary Table S1, left column). It can clearly be seen that increasing incubation time leads to a slower catalytic rate. Inhibition is stronger and slightly faster for higher inhibitor concentrations, which is in good agreement with reported experimental findings [15, 25].

The implemented model modifications are also based on molecular considerations. The reaction center of wild-type RuBisCO can be assumed to be optimally adapted for RuBP

enolization, which is therefore expected to proceed fast in contrast to XuBP enolization. This is due to the positioning of the carbamylated lysine residue (KCX): For RuBP, KCX is capable of removing a hydrogen from the C3 carbon, initiating enolization. This is not the case for XuBP, since the respective hydrogen is on the opposite side of the molecule. Another mechanism has to be employed for enolizing XuBP, which up to now has yet to be revealed. However, a recent small quantum chemical model of the RuBisCO active site [21] proposed a promising interpretation of a water molecule being bound to Mg^{2+}, which may well be a candidate for being a (probably less efficient) hydrogen acceptor.

The different states arising directly after the enolization of XuBP and RuBP reflect the same bound molecule but a different spatial arrangement of the catalyzing enzyme. In particular, they are different with respect to the positions of hydrogens close to the Mg^{2+} center. While for RuBP we find a hydrogen bound to the KCX residue, this is not the case for the situation after XuBP enolization. The state arising after enolization of RuBP is catalytically active, since this configuration facilitates protonation of the oxygen atom at RuBP position 2, and hydration of the carboxylated intermediate. Because this is not the case after enolization of XuBP, the resulting intermediate state is catalytically inactive. Since only hydrogen positions are different in the two states, it is plausible to assume that the states can be converted into each other by rearrangement of the hydrogen atoms facilitated by the various hydrogen donors and acceptors present in the molecular environment. A pictorial representation of the two different situations is given in Fig. 8.

To account for the experimentally observed decline in activity during carboxylation of XuBP, it was necessary to include another inhibitor in the model description. The observed decline suggests that this inhibitor is formed from an intermediate state that arises after binding of XuBP but before transformation of the inactive to the active enediol intermediate state. Decline in XuBP carboxylation activity cannot be explained by inhibitors formed from intermediates of the main catalytic pathways (represented by bold reaction arrows in Figs. 1 and 6), because under XuBP carboxylating conditions, most enzyme is bound in intermediate complexes (EI1 and EE2) of the slow supply pathway. Therefore, side reactions diverging from the main pathway can only exert a minor influence on the overall system's dynamics. A good candidate for the missing slowly formed inhibitor is deoxypentodiulose phosphate (DP1P), which may result from the enediol intermediate by β-elimination at an even slower rate than the production of XuBP (see [15, 11]). The exact mechanism of the β-elimination is as yet unconfirmed. However, in the simplest case, the O3 atom of the enediol would have to lose a proton (probably to its hydrogen bond partner His-294), and then the rest of the reaction would occur completely independent from the protein environment. The low efficiency of this reaction underlines the weak, if any support by the molecular environment. Thus, it can be argued that the β-elimination is not critically influenced by the location of the hydrogen atoms that discerns the two enediol intermediate states EE1 and EE2 and it is plausible to assume that DP1P may be produced from both of these intermediates.

A typical simulation for the kinetics of XuBP carboxylation for wildtype RuBisCO is depicted in Fig. 9A. The bold line indicates the rate of carboxylation (left axis). The concentrations of the intermediate enzyme-substrate complexes are normalized to the total amount of enzyme (dashed lines, right axis). A striking feature is the relatively slow initial increase of the catalytic rate. The time courses of the three intermediates before and after enolization (EI1 and EE2, respectively) and after β-elimination (EDP2) demonstrate the three time scales on which XuBP carboxylation occurs. Binding of the

substrate is fast (dashed blue line) while the enolization is considerably slower and leads to a maximal concentration of the enediol intermediate after 200 seconds (dashed green line). The formation of the secondary inhibitor DP1P proceeds on an even slower time scale and formation and release are balanced after around 1000 seconds. The concerted interaction of these processes result in the overall dynamic behavior that carboxylation reaches a maximal rate $v_{\max}$ after time $T_{\max}$. The apparent fallover extent is determined by $f^{\text{app}} = 1 - v_f/v_{\max}$, where v_f denotes the final catalytic activity. An apparent halftime $T_{1/2}$ (see Fig. 9A) was determined numerically. We have performed a sensitivity analysis to determine which rate constants are most influential on these characteristic quantities. The result is depicted in Fig. 9B. Here, for all relevant parameters, the corresponding response coefficients for the characteristic observables $T_{\max}$, $v_{\max}$, f^{app} and $T_{1/2}$ are given. All other parameters exert only a marginal influence on these dynamic properties (the complete list in given in Supplementary Table S3). It is confirmed that the dynamics is dominated by the rates of enolization (k^+_{EE2}) of XuBP, the formation of a secondary inhibitor by β-enolization (k_{EDP2}) and its release (k^-_{D2}). In particular, the time $T_{\max}$ to reach maximal activity is reduced if either the rate of enolization or the β-elimination is increased. Increase of the former will also lead to an increase of the maximal activity $v_{\max}$ while increase of the latter will result in its decrease. Both rates exert a positive control on the observed apparent fallover extent f^{app} and a negative control on the observed half-time. The rate of back-transformation (k^-_{SW}) of the enediol intermediate has a strong positive control on the maximal activity but not on the other characteristic parameters. Similarly to fallover on RuBP, which was discussed above, increasing the rate of inhibitor release (k^-_{D2}) will diminish fallover while simultaneously reducing its the half-time.

A single amino acid exchange disrupts the molecular mechanisms

In a particularly interesting tobacco RuBisCO mutant the active site Leu-335 is replaced by valine, which means that the aliphatic amino acid is shortened by one CH_2-group. This mutation considerably changes the spatial arrangement of loop 6 of the RuBisCO large subunit which plays an important role in keeping the active site closed during the reaction. The actual main interaction partners of Leu-335 are Phe-127 (of the other L subunit) and the aliphatic part of Lys-334. Both interactions will be affected, since without a rearrangement of the protein backbone, the Val-335 is unable to reach both residues. Fig. 10 displays this situation in greater detail. Since Lys-334 is participating in the closing of the active site, it is therefore reasonable to assume that the release of any molecule bound to the active site is facilitated [15].

As a result, in contrast to wildtype RuBisCO, the Val-335 mutant is not susceptible to fallover during carboxylation of RuBP. Further, pre-incubation of the Val-335 mutant with XuBP does not appear to increase the inhibitory effect [15]. While this Val-335 mutant exhibits a drastically reduced carboxylation rate on RuBP (about sixfold), it catalyzes the poor substrate XuBP roughly twice as fast as the wild-type form. Curiously, when XuBP is applied as a substrate to the Val-335 mutant, the catalytic activity is slowly increasing over time, a scenario that may be described as inverse fallover. A parameter set resembling the Val-335 mutant is given in the Supplementary Table S1 (right column) and a simulation of the kinetics on XuBP as substrate is depicted in Fig. 11A.

Two main differences are responsible for the drastically different modes of behavior. Firstly, the Val-335 mutant releases the inhibitors XuBP and DP1P considerably faster,

thus the binding sites are quickly freed and ready to bind new substrate. This difference also explains why for this mutant no fallover on RuBP under anaerobic conditions is observed. The second distinction is that in the mutant form enolization of XuBP and RuBP proceed on similar time scales and that they operate near equilibrium. In the wild type form RuBP enolization is enhanced by the carbamylated lysine (KCX) residue. Any mutation which disturbs the balanced substrate position near KCX will therefore automatically reduce the RuBP enolization and cause reduced enediol stability. This in turn implies that enolization may be reversed and RuBP released.

Compared to the wild type form, Val-335 RuBisCO rapidly adapts a quasi steady state carboxylation rate v^*, since equilibration of substrate binding and enolization are fast. The increase in activity shown in the time course of Fig. 11A reflects the equilibration of the binding of free enzyme to the released substrate. This is illustrated by the flux through reaction v_{EE1} in reverse direction depicted by the black curve in Fig. 11A and the concentration of free RuBP (dashed blue line).

At first, the explanation of an increased rate by equilibration with the native substrate seems counter-intuitive. However, an estimation demonstrates that this assumption is not unrealistic: The initial increase of RuBP in Fig. 11A suggests a release rate of approximately one RuBP molecule per catalytic site per 5000 seconds. This lies in the same order of magnitude as the carboxylation rate. An analysis of the control that various parameters exert on this apparent inverse fallover is depicted in Fig. 11B and reflects the distinctions of the model dynamics. Similar to the wild type form, control over the time T^* is exclusively exerted by those rates within the XuBP branch ($k_X^{+/-}$, $k_{EE2}^{+/-}$ and k_{SW}^{-}) of the reaction scheme (Fig. 6). The corresponding rate v^* is also predominantly influenced by these rates. Interestingly, the control of halftime and extent of the slow increase in catalytic rate is spread among rate parameters from the main catalytic pathway and the secondary branch. All parameters not mentioned in the diagram in Fig. 11B only negligibly influence the dynamics (for a full list of response coefficients, see Supplemetary Table S4).

Discussion

We have presented mathematical models that quantitatively reflect various experimentally observed characteristics of RuBisCO. The models were held as simple and general as possible in order to serve as a theoretical framework which allows to investigate the dynamic properties of any type of RuBisCO under different conditions. The simplicity of the models strongly facilitates the identification of key parameters and simplifies fitting to experimental data.

RuBisCOs other than type IB found in higher plants do not display fallover (the slow inactivation due to inhibitor formation) *in vitro*. Among these, there are considerable differences in Michaelis constants, maximal activity and CO_2/O_2-specificity [29, 11, 35]. Our mathematical analysis suggests that some of the differences may be explained by a different degree of stability of intermediate enzyme-substrate complexes. An elevated energy level of the intermediate arising from the binding of CO_2 to the enediol intermediate, for example, leads to an increased Michaelis constant for CO_2 but simultaneously to an increased maximal catalytic activity for excess CO_2. We conclude that this difference in energetic configuration is the main explanation for the observed kinetic constants in

RuBisCO from *Synechococcus*. We assume that the distinct properties are an outcome of the differing selective pressures during the evolutionary history of free cyanobacteria and higher plants, respectively. In line with the results presented in [35], it can be argued that a lower affinity to CO_2 but a higher maximal activity is favorable under environments with a high average or rapidly fluctuating CO_2 concentration. The oxygenation activity of RuBisCO results in a net reduction of the carbon fixation efficiency and it seems plausible that selective pressures favored the reduction of this side reaction. In fact, the observation that affinities to oxygen and maximal oxygenation rates are rather constant among species suggests that the molecular evolution of RuBisCO has minimized this side reaction and that a further reduction is difficult, if not impossible.

A common feature of all investigated RuBisCOs from higher plants is that they are slowly inactivated during *in vitro* assays. Our mathematical considerations demonstrated that the formation of two inhibitors is sufficient to explain the fallover on the prime substrate RuBP quantitatively for various external CO_2 and O_2 concentrations, thus confirming the suggestions in [10, 15] that XuBP and PDBP are the critical self-produced inhibitors responsible for the slow activity decline. They are formed by misprotonation from the enediol intermediate or by H_2O_2 elimination of the peroxyketone intermediate, respectively. The characeteristic times of these processes define the two time scales on which fallover occurs.

Experimental evidence presented in [15] suggest the formation of another inhibitor, DP1P, resulting from β-elimination of the enediol intermediate. While this side reaction was not necessary for explaining the two time scales of fallover, its inclusion presents a critical model refinement, allowing to explain the observed carboxylation dynamics on the secondary substrate XuBP. Supported by the molecular structure around the catalytic site, our model results strongly support an alternative enolization mechanism that has not been described previously.

Within the green kingdom of green algae and higher plants, the active center of RuBisCO is highly conserved, regarding amino acid sequences as well as three dimensional structure. An interesting mutant form is induced by the single amino acid exchange Leu→Val at position 335. This mutant displays totally different dynamic properties than the wild-type form. Whereas the maximal activity on RuBP is reduced, it does not show any signs of fallover. It not only works faster on XuBP than wild-type, the catalytic activity seems to exert a slow increase over time. With a suitable parameter set, our model is capable to reflect these characteristics and our investigations suggest that the activity increase results from the equilibration with the slowly released native substrate RuBP. Interestingly, the parameters used for the Val-335 mutant and wild-type do not differ significantly in the later reaction steps beginning with carboxylation or oxygenation of the enediol intermediates, which indicates that the altered activity results largely from disturbed substrate binding, enolization and orientation of the enediol intermediate. Collectively, evidences solidify the idea that loosening of the active site alleviates or abolishes fallover whereas loosening can be induced either by a structural variation like in the loop 6 mutant [15] or by increased temperature [12]. Both alterations lead to an increased inhibitor production, but the concomitant faster release of inhibitors reduces fallover extent and rate. This suggests that the difference between fallover and non-fallover RuBisCOs might not be the property of inhibitor production, but rather the ability to convert or release inhibitors efficiently, as predicted by our calculations. That idea is in accordance with increased production of H_2O_2 and in that of PDBP by *Chlamydomonas reinhardtii*

and *R.Rubrum* RuBisCO [42] without attendant fallover in carboxylation. Pearce et al. [11] also affirm that inhibitors produced by *Synechococcus*, *Galdieria sulfuraria* and *R. rubrum* RuBisCO are not inhibitory under substrate-saturated conditions. It is often stated that fallover RuBisCOs show a higher specificity for CO_2 which prompted Pearce et al. [15] to speculate that the greater carboxylase activity comes at the cost of making the closure of loop 6 over the substrate so precise that substrate analogues cannot escape from the active site easily. Indeed, the specificity factor Ω is decreasing constantly with increasing temperature in spinach RuBisCO [43] which is supposed to be caused by active site loosening. However, the role of structural changes in loop 6 for fallover is possibly overestimated, because many more residues, for example also from the other large subunit in the L2 dimer, extend into the active site. Moreover, the sequence VVGKLEG of loop 6 is highly conserved throughout all eukaryotes [6], including fallover and non-fallover RuBisCOs. Based on these considerations it would be worth to analyze and compare greater parts of the active site to understand the structural foundation of fallover. Apart from inhibitor release or further conversion to less tightly binding species, our model results suggest that inhibitor back-conversion also contributes to fallover alleviation.

Another interesting mutant form is resulting from a single amino acid exchange (E48Q) from RuBisCO of *R. rubrum*. In its wildtype form, the L2 configuration does not display fallover, but a comparably fast production of one XuBP in approximately 70 catalytic cycles [44]. The mutant form, however, is missing a contact between a glutamate residue (position 48) and the Lys-329 (corresponding to Lys-334 in tobacco) and produces XuBP in a ratio of 19 vs. 25 normal products, i. e. the sum of carboxylation and oxygenation products [44]. Similar to the case of the Val-335 mutant of wild-type tobacco, our theory suggests that due to the lowered catalytic efficiency RuBP is more likely to participate in other reactions inside RuBisCO, leading to more side products such as XuBP.

Our findings have potential impact on the various attempts (for a review, see [45]) to improve the carbon fixation abilities of crop plants by targeted genetic approaches. With the presented theoretical background, processes can be identified whose alteration will most strongly influence the targeted property. Simultaneously, 'side-effects' can be predicted by simulating the overall kinetic behavior.

Methods

Model formulation

Mathematical models to describe the kinetic behavior of RuBisCO have been developed according to Figs. 1 and 6. In this paper, only reaction kinetics for fully activated RuBisCO is considered. Therefore, binding of non-substrate CO_2 to an active-site lysine residue and stabilization of the lysyl-carbamate by subsequent binding of Mg^{2+} is not included in the models.

The first, simpler model describes the accumulation and depletion of the free enzyme concentration E and the enzyme-substrate complexes ER, ERC, ERO as well as the enzyme-inhibitor complexes EI1 and EI2 (see Fig. 1 for a detailed explanation). The second model, which focuses on the behavior of RuBisCO when using the secondary substrate XuBP, further includes the species EE1, EE2, describing intermediary enzyme-substrate complexes, and EDP1 and EDP2, describing additional enzyme-inhibitor complexes (see

Fig. 6). Further, the concentration of ribulose-1,5-bisphosphate (RuBP) is considered a variable since the accumulation of the free primary substrate is important to explain the dynamic properties.

Each species is produced and consumed by elementary processes, defining how its concentration changes with time. For binding processes, the forward rates describe the rates of association of enzyme-ligand complexes and the reverse rates describe the rates of dissociation. For example, for the complex ERC, which represents the enzyme complex after binding of substrate CO_2, mass balance yields

$$\frac{d[ERC]}{dt} = v^+_{ERC} - v^-_{ERC} - v_{cat}. \tag{5}$$

Here, the rates v describe the turnover rates of the elementary processes and the superscripts + and − denote forward and reverse, respectively. For example, v^+_{ERC} denotes the rate of binding the second substrate CO_2 while v^-_{ERC} denotes the dissociation rate. For the elementary processes, we assume simple mass-action kinetics, yielding the following descriptions:

$$v^+_{ERC} = k^+_{ERC}[ER][CO_2] \quad \text{and} \quad v^-_{ERC} = k^-_{ERC}[ERC], \tag{6}$$

where the dimension of binding rate constants is $\mu\mathrm{M}^{-1}\mathrm{s}^{-1}$ and the dimension of dissociation rate constants and all other rate constants is s^{-1}.

The rates of the final steps in which the substrates (two PGA in the case of the carboxylating pathway, one PGA and one PG in the oxygenation pathway) are released, are considered irreversible and described by

$$v_{cat} = k_{cat}[ERC] \quad \text{and} \quad v_{oxy} = k_{oxy}[ERO]. \tag{7}$$

For the simple model (Fig. 1), this results in a mathematical model of five coupled differential equations with 16 rate parameters. In the detailed model (Fig. 6), we get 10 coupled ordinary differential equations containing 26 rate parameters. The full list of equations is given in the Supplementary Text S1 and S3.

Quasi steady state approximation

To arrive at a reduced system describing the fallover dynamics, a quasi steady state approximation for the variables involved in fast reactions (bold reaction arrows in Fig. 1) has been performed. For this, the algebraic equation system

$$d[ER]/dt = 0 \tag{8}$$
$$d[ERC]/dt = 0 \tag{9}$$
$$d[ERO]/dt = 0 \tag{10}$$

was solved to yield the analytic expressions for the variables $[ER], [ERC]$ and $[ERO]$. These expressions were used to eliminate the three fast variables from the full system equations to result in a reduced system of two coupled linear differential equations. From this reduction, we obtained equations for the initial state of the system which corresponds to a quasi steady state that is characterized by an inhibitor level close to zero. From these equations, we derived analytic expressions relating experimentally accessible quantities, in particular K_M, $V^{\max}$ and substrate specificity values to the rate parameters or defined

combinations thereof. Secondly, the simplified equation system was used to relate the slow rate variables to the observable quantities describing the fallover effect, i. e. the fallover extent and the characteristic time. The detailed calculations are given in Supplementary Text S2.

Determining the fast parameters from K_M- and $V^{\max}$- values

The most important formulas to connect observed quantities with model parameters are summarized in the following. The expression for the initial concentration of ER allows to derive analytic formulas for the carboxylation and oxygenation rates v^i_{cat} and v^i_{oxy} which are observed immediately after initiation of the assays. These were used to derive theoretical expressions for the K_M and $V^{\max}$ values. These expressions are derived by considering the limit case for infinitely large substrate concentrations. For example, for the saturating carboxylation rate $V^{\max}_{\text{carb}}$, the following relation holds:

$$V^{\max}_{\text{carb}} = \lim_{[RuBP],[CO_2]\to\infty} v^i_{cat} = k_{cat}E^{\text{tot}}. \tag{11}$$

To determine the K_M-value for one substrate, only the limit of infinite concentration of the other substrate has to be considered. Thus

$$\lim_{[CO_2]\to\infty} v^i_{cat} = \frac{V^{\max}_{\text{carb}}[RuBP]}{[RuBP] + K_{M(\text{RuBP})}}, \tag{12}$$

which yields

$$K_{M(\text{RuBP})} = \frac{k_{cat}}{k^+_{ER}}. \tag{13}$$

Similarly,

$$K_{M(\text{CO}_2)} = \frac{1}{\gamma}(1 + \omega[O_2]), \tag{14}$$

where $\gamma = k^+_{ERC}/(k^-_{ERC} + k_{cat})$ and $\omega = k^+_{ERO}/(k^-_{ERO} + k^+_{EI2} + k_{oxy})$. In agreement with experimental findings [29], the K_M-value for CO_2 is dependent on the ambient oxygen concentration and is larger for aerobic than for anaerobic conditions.

Applying analogous considerations for the saturating oxygenation rate $V^{\max}_{\text{ox}}$ yields

$$V^{\max}_{\text{ox}} = k_{oxy}E^{\text{tot}} \tag{15}$$

and

$$K_{M(\text{O}_2)} = \frac{1}{\omega}(1 + \gamma[CO_2]). \tag{16}$$

A characteristic experimental quantity for different RuBisCOs is the relative substrate specificity Ω which is defined as the ratio of the carboxylation versus oxygenation rate under the condition that carbon dioxide and oxygen are present in the same concentration [46]. Inserting equal concentrations into the expressions for v^i_{cat} and v^i_{oxy} yields

$$\Omega = \frac{k_{cat}\gamma}{k_{oxy}\omega}. \tag{17}$$

This set of equations is useful in two respects. Firstly, it provides insight into which parameters and parameter combinations are determinants of the observed key characterstics such as $V^{\max}$-values, K_M-values and substrate specificity. Secondly, it allows to

determine these parameters or parameter combinations directly from only a relatively small number of experimentally determined quantities. For example in [29] and [11], K_M-values, maximal catalytic activities and substrate specificities are given for RuBisCOs extracted from a wide range of species. Application of Eqs. 11 and 13–17 directly yields the rate parameters k_{cat}, k_{oxy}, k^+_{ER} as well as the derived parameters γ and ω. Knowledge of the latter two quantities restricts the freedom of choice for the remaining parameters, thus considerably facilitating the fit of the fast rate constants to experimental data.

Determination of fallover related parameters

The simplified equation system resulting from the quasi steady state approximation (Eqs. 8–10) allows to derive a closed expression for the fallover extent. The extent is defined as the relative loss of activity from the initial rate v^i_{cat}, after the final rate v^f_{cat} has been reached (in the theoretical limit $t \to \infty$). With good accuracy, the approximation formula

$$f = 1 - \frac{v^f_{cat}}{v^i_{cat}} \approx \frac{\Gamma_1 + \Gamma_2 \omega [O_2]}{1 + \Gamma_1 + \left(1 + \frac{k_{cat}}{k^+_{ER}[RuBP]}\right)\gamma[CO_2] + \left(1 + \Gamma_2 + \frac{k_{oxy}}{k^+_{ER}[RuBP]}\right)\omega[O_2]} \tag{18}$$

holds, where the abbreviations

$$\Gamma_1 = \frac{k^+_{EI1}}{k^-_{EI1} + k^-_X} \quad \text{and} \quad \Gamma_2 = \frac{k^+_{EI2}}{k^-_{EI2} + k^-_P} \tag{19}$$

have been introduced. This analytic expression provides insight into which parameters and parameter combinations are critically influencing the observed fallover extent. Simultaneously, it demonstrates how experimental data on the fallover extent under different conditions can be exploited to draw conclusions about the system parameters.

Eq. 18 assumes a particularly simple form for the anaerobic case ($[O_2] = 0$). After determination of the rate constants k^+_{ER} and k_{cat} as well as the derived paramter γ from experimental K_M and $V^{\max}$-values (see above), knowledge of the fallover extent under oxygen-free conditions allows the calculation of Γ_1. Once this derived parameter is known, Γ_2 may be calculated from the fallover extent under aerobic conditions after determination of k_{oxy} and ω from experimental K_M- and specificity values.

Exploiting measured fallover half times is more difficult. A simple relation to the system parameters can only be derived for the anaerobic case. For $[O_2] = 0$, the oxygenation pathway is non existent and therefore only inhibitor EI_1 is formed. In this case, the dynamics of inhibitor formation result from the simple solution of a single linear differential equation, yielding

$$[EI1](t) = [EI1]^f (1 - e^{-\lambda t}), \tag{20}$$

with $[EI1]^f$ denoting the final concentration of inhibitor EI1 and

$$\lambda = a k^+_{EI1} + k^-_{EI1} + k^-_X, \tag{21}$$

where a depends on various parameters and external substrate concentrations (for details, see Supplementary Text S2). The value λ corresponds to the observed fallover rate k_{obs}, and is related to the observed half-time $T_{1/2}$ by

$$\lambda = k_{\text{obs}} = \frac{\ln 2}{T_{1/2}}. \tag{22}$$

Under aerobic conditions, inhibitor accumulation and loss of activity is mathematically described by the solution of two coupled linear differential equations with the general form

$$v_{cat}(t) = v_{cat}^{f} + c_1 e^{-\lambda_1 t} + c_2 e^{-\lambda_2 t}. \tag{23}$$

The parameters λ_1 and λ_2 correspond to the eigenvalues of the reduced system matrix. By visual inspection, the superposition of two exponential curves is often hard to distinguish from a simple exponential decay. Therefore it is difficult to obtain reliable hints about the system parameters from the observed characteristic times under aerobic conditions. However, if $T_{1/2}$ is the observed half-time, the relation

$$\frac{\ln 2}{\max(|\lambda_1|, |\lambda_2|)} \leq T_{1/2} \leq \frac{\ln 2}{\min(|\lambda_1|, |\lambda_2|)} \tag{24}$$

must hold.

Numerical determination of response coefficients

The response coefficient of a certain quantity X on a parameter p describes the response of the quantity upon a small change in the parameter. It is defined (see for example [47]) as the ratio of the fold change in X to the fold change in p for small variations,

$$R_p^X = \lim_{\Delta p \to 0} \frac{\Delta X/X}{\Delta p/p} = \frac{p}{X}\frac{\partial X}{\partial p} = \frac{\partial \ln X}{\partial \ln p}. \tag{25}$$

For the response coefficients on the fallover extent, the following summation theorem can be proven (see Supplementary Text S4):

$$\sum_i R_{k_i}^f = 0. \tag{26}$$

For characteristic times $T_{\max}$, $T_{1/2}$ and T^*, the summation theorem

$$\sum_i R_{k_i}^T = -1 \tag{27}$$

holds true and for quantities with the dimension s^{-1} ($v_{\max}$, v^*, k_{obs}), the relation

$$\sum_i R_{k_i}^v = 1 \tag{28}$$

holds.

These theoretical summation theorems serve as a good test whether numerical accuracy is sufficient. In all determined sets of response coefficients the summation theorems were observed with a deviation of less than 10^{-3}, indicating a very good accuracy.

Acknowledgements

J.G. would like to thank Prof. Inger Andersson (Biomedical Centre, Uppsala) for providing a full wildtype hexadecamer *C. reinhardtii* RuBisCO structure. The authors thank Prof. Peter Saalfrank for critically reading the manuscript.

Funding

This work was funded by the German Federal Ministry of Education and Research through the Systems Biology Research Initiative "*Go*FORSYS" as well as the "FORSYS"-Partner program (grant number 0315261) and the Scottish Universities Life Science Alliance (SULSA).

References

[1] Portis, A. R. and Parry, M. A. J. (2007) Discoveries in Rubisco (Ribulose 1,5-bisphosphate carboxylase/oxygenase): a historical perspective. Photosynth Res **94**(1), 121–143

[2] Jensen, R. G. and Bahr, J. T. (1977) Ribulose 1,5-Bisphosphate Carboxylase-Oxygenase Annual Review of Plant Physiology **28**(1), 379–400

[3] Tabita, F. (1999) Microbial ribulose 1,5-bisphosphate carboxylase/oxygenase: A different perspective PHOTOSYNTHESIS RESEARCH **60**(1), 1–28

[4] Andersson, I. and Taylor, T. C. (2003) Structural framework for catalysis and regulation in ribulose-1,5-bisphosphate carboxylase/oxygenase. Arch Biochem Biophys **414**(2), 130–140

[5] Andersson, I. (2008) Catalysis and regulation in Rubisco. J Exp Bot **59**(7), 1555–1568

[6] Andersson, I. and Backlund, A. (2008) Structure and function of Rubisco. Plant Physiol Biochem **46**(3), 275–291

[7] Edmondson, D. L., Badger, M. R. and Andrews, T. J. (1990) A Kinetic Characterization of Slow Inactivation of Ribulosebisphosphate Carboxylase during Catalysis. Plant Physiol **93**(4), 1376–1382

[8] Edmondson, D. L., Badger, M. R. and Andrews, T. J. (1990) Slow Inactivation of Ribulosebisphosphate Carboxylase during Catalysis Is Not Due to Decarbamylation of the Catalytic Site. Plant Physiol **93**(4), 1383–1389

[9] Edmondson, D. L., Badger, M. R. and Andrews, T. J. (1990) Slow Inactivation of Ribulosebisphosphate Carboxylase during Catalysis Is Caused by Accumulation of a Slow, Tight-Binding Inhibitor at the Catalytic Site. Plant Physiol **93**(4), 1390–1397

[10] Kim, K. and Portis, A. R. (2006) Kinetic analysis of the slow inactivation of Rubisco during catalysis: effects of temperature, O2 and Mg(++). Photosynth. Res. **87**(2), 195–204

[11] Pearce, F. G. (2006) Catalytic by-product formation and ligand binding by ribulose bisphosphate carboxylases from different phylogenies. Biochem J **399**(3), 525–534

[12] Schrader, S. M., Kane, H. J., Sharkey, T. D. and von Caemmerer, S. (2006/10/02) High temperature enhances inhibitor production but reduces fallover in tobacco Rubisco Functional Plant Biology **33**(10), 921–929

[13] Robinson, S. P. and Portis, A. R. (1989) Ribulose-1,5-bisphosphate carboxylase/oxygenase activase protein prevents the in vitro decline in activity of ribulose-1,5-bisphosphate carboxylase/oxygenase. Plant Physiol **90**(3), 968–971

[14] Portis, A. R. (2003) Rubisco activase - rubisco's catalytic chaperone. Photosynth Res **75**(1), 11–27

[15] Pearce, F. G. and Andrews, T. J. (2003) The relationship between side reactions and slow inhibition of ribulose-bisphosphate carboxylase revealed by a loop 6 mutant of the tobacco enzyme. J Biol Chem **278**(35), 32526–32536

[16] Farquhar, G. D. (1979) Models describing the kinetics of ribulose biphosphate carboxylase-oxygenase. Arch Biochem Biophys **193**(2), 456–468

[17] Yokota, A., Wadano, A. and Murayama, H. (1996) Modeling of continuously and directly analyzed biphasic reaction courses of ribulose 1,5-bisphosphate carboxylase/oxygenase. J Biochem **119**(3), 487–499

[18] King, W. A., Gready, J. E. and Andrews, T. J. (1998) Quantum chemical analysis of the enolization of ribulose bisphosphate: the first hurdle in the fixation of CO2 by Rubisco. Biochemistry **37**(44), 15414–15422

[19] Mauser, H., King, W. A., Gready, J. E. and Andrews, T. J. (2001) CO(2) fixation by Rubisco: computational dissection of the key steps of carboxylation, hydration, and C-C bond cleavage. J Am Chem Soc **123**(44), 10821–10829

[20] McNevin, D., von Caemmerer, S. and Farquhar, G. (2006) Determining RuBisCO activation kinetics and other rate and equilibrium constants by simultaneous multiple non-linear regression of a kinetic model. J. Exp. Bot. **57**(14), 3883–3900

[21] Kannappan, B. and Gready, J. E. (2008) Redefinition of Rubisco Carboxylase Reaction Reveals Origin of Water for Hydration and New Roles for Active-Site Residues J. Am. Chem. Soc. **130**(45), 15063–15080

[22] Edmondson, D. L. (1990) Substrate Isomerization Inhibits Ribulosebisphosphate Carboxylase-Oxygenase During Catalysis FEBS Letters **260**, 62–66

[23] Lorimer, B. (1976) The Activation of Ruibulose-1,5-bisphosphate Carboxylase by Carbon Dioxide and Magnesium Ions. Equilibria, Kinetics, a Suggested Mechanism, and Physiological Implications Biochemistry **15**, 529–536

[24] Zhu, G. and Jensen, R. G. (1991) Fallover of Ribulose 1,5-Bisphosphate Carboxylase/Oxygenase Activity : Decarbamylation of Catalytic Sites Depends on pH. Plant Physiol **97**(4), 1354–1358

[25] McCurry, S. D. and Tolbert, N. E. (1977) Inhibition of ribulose-1,5-bisphosphate carboxylase/oxygenase by xylulose 1,5-bisphosphate. J Biol Chem **252**(23), 8344–8346

[26] Harpel, M. R., Serpersu, E. H., Lamerdin, J. A., Huang, Z. H., Gage, D. A. and Hartman, F. C. (1995) Oxygenation mechanism of ribulose-bisphosphate carboxylase/oxygenase. Structure and origin of 2-carboxytetritol 1,4-bisphosphate, a novel O2-dependent side product generated by a site-directed mutant. Biochemistry **34**(35), 11296–11306

[27] von Caemmerer, S. (2000) Biochemical Models of Leaf Photosynthesis - Techniques in Plant Sciences Series Number 2 CSIRO PUBLISHING, Collingwood, Australia

[28] Frank, J. (1998) Thermodynamics and kinetics of sugar phosphate binding to D-ribulose 1,5-bisphosphate carboxylase/oxygenase (RUBISCO) J.Chem.Soc. , Faraday Trans. **94 (15)**, 2127–2133

[29] Whitney, S. M., Baldet, P., Hudson, G. S. and Andrews, T. J. (2001) Form I Rubiscos from non-green algae are expressed abundantly but not assembled in tobacco chloroplasts. Plant J **26**(5), 535–547

[30] Morell, M. K., Paul, K., O'Shea, N. J., Kane, H. J. and Andrews, T. J. (1994) Mutations of an active site threonyl residue promote beta elimination and other side reactions of the enediol intermediate of the ribulosebisphosphate carboxylase reaction. J Biol Chem **269**(11), 8091–8098

[31] Read, B. A. and Tabita, F. R. (1994) High substrate specificity factor ribulose bisphosphate carboxylase/oxygenase from eukaryotic marine algae and properties of recombinant cyanobacterial RubiSCO containing "algal" residue modifications. Arch Biochem Biophys **312**(1), 210–218

[32] Morell, M. K., Kane, H. J., Hudson, G. S. and Andrews, T. J. (1992) Effects of mutations at residue 309 of the large subunit of ribulosebisphosphate carboxylase from Synechococcus PCC 6301. Arch Biochem Biophys **299**(2), 295–301

[33] Terzaghi, B. E., Laing, W. A., Christeller, J. T., Petersen, G. B. and Hill, D. F. (1986) Ribulose 1,5-bisphosphate carboxylase. Effect on the catalytic properties of changing methionine-330 to leucine in the Rhodospirillum rubrum enzyme. Biochem J **235**(3), 839–846

[34] Kane, H., Viil, J., Entsch, B., Paul, K., Morell, M. and Andrews, T. (1994) An Improved Method for Measuring the CO2/O2 Specificity of Ribulosebisphosphate Carboxylase-Oxygenase. Australian Journal of Plant Physiology **21**, 449–461

[35] Tcherkez, G. G. B., Farquhar, G. D. and Andrews, T. J. (2006) Despite slow catalysis and confused substrate specificity, all ribulose bisphosphate carboxylases may be nearly perfectly optimized. Proc Natl Acad Sci U S A **103**(19), 7246–7251

[36] Gutteridge, S. and Pierce, J. (2006) A unified theory for the basis of the limitations of the primary reaction of photosynthetic CO(2) fixation: was Dr. Pangloss right? Proc Natl Acad Sci U S A **103**(19), 7203–7204

[37] Kane, H., Wilkin, J., Portis, A. and Andrews, T. (1998) Potent inhibition of ribulosebisphosphate carboxylase by an oxidized impurity in ribulose-1,5-bisphosphate Plant Physiol **117**(3), 1059–1069

[38] Zhu, G., Bohnert, H., Jensen, R. and Wildner, G. (1998) Formation of the tight-binding inhibitor, 3-ketoarabinitol-1,5-bisphosphate by ribulose-1,5-bisphosphate carboxylase/oxygenase is O-2-dependent Photosynth. Res. **55**(1), 67–74

[39] Portis, A. R., Lilley, R. M. and Andrews, T. J. (1995) Subsaturating Ribulose-1,5-Bisphosphate Concentration Promotes Inactivation of Ribulose-1,5-Bisphosphate Carboxylase/Oxygenase (Rubisco) (Studies Using Continuous Substrate Addition in the Presence and Absence of Rubisco Activase). Plant Physiol **109**(4), 1441–1451

[40] Yokota, A. (1991) Carboxylation and Detoxification of Xylulose Bisphosphate by Spinach Ribulose Bisphosphate Carboxylase Oxygenase Plant & cell physiology **32**(6), 755–762

[41] Zhu, G. and Jensen, R. G. (1991) Xylulose 1,5-Bisphosphate Synthesized by Ribulose 1,5-Bisphosphate Carboxylase/Oxygenase during Catalysis Binds to Decarbamylated Enzyme. Plant Physiol **97**(4), 1348–1353

[42] Kim, K. and Portis, A. R. (2004) Oxygen-dependent H2O2 production by Rubisco. FEBS Lett **571**(1-3), 124–128

[43] Jordan, D Ogren, W. (1984) The CO2/O2 Specificty of Ribulose 1,5-Bisphosphate Carboxylase Oxygenase - Dependence on Ribulosebisphosphate Concentration, pH and Temperature Planta **161**(4), 308–313

[44] Lee, E. H., Harpel, M. R., Chen, Y. R. and Hartman, F. C. (1993) Perturbation of reaction-intermediate partitioning by a site-directed mutant of ribulose-bisphosphate carboxylase/oxygenase. J Biol Chem **268**(35), 26583–26591

[45] Parry, M. A. J., Andralojc, P. J., Mitchell, R. A. C., Madgwick, P. J. and Keys, A. J. (2003) Manipulation of Rubisco: the amount, activity, function and regulation. J Exp Bot **54**(386), 1321–1333

[46] Laing, W. A. (1974) Regulation of Soybean Net Photosynthetic CO(2) Fixation by the Interaction of CO(2), O(2), and Ribulose 1,5-Diphosphate Carboxylase. Plant Physiol **54**(5), 678–685

[47] Heinrich, R. and Schuster, S. (1996) The Regulation of Cellular Systems Chapman & Hall, London, England

[48] Taylor, T. C., Backlund, A., Bjorhall, K., Spreitzer, R. J. and Andersson, I. (2001) First Crystal Structure of Rubisco from a Green Alga, Chlamydomonas Reinhardtii J Biol Chem **276**(51), 48159–48164

Supplementary Material

Text S1 – Model equations for the simple model
Text S2 – Quasi steady state approximation
Text S3 – Model equations for the simple model
Text S4 – Summation theorems for response coefficients

Table S1 – Parameters for wild-type and Val-335 RuBisCO from tobacco for the extended model
Table S2 – Response coefficients for fallover extent and characteristic time under anaerobic and aerobic conditions
Table S3 – Response coefficients for fallover extent and characteristic time on XuBP as substrate for wildtype RuBisCO
Table S4 – Response coefficients for fallover extent and characteristic time on XuBP as substrate for the Val-335 mutant

Table 1: Measured and calculated parameter values for RuBisCOs from different species.

	Tobacco[a]	*G. sulfuraria*[a]	*P. tricornutum*[a]	*G. monilis*[a]	*Synechococcus*	*R. rubrum*
Experimental data						
$V_{\max}$/active site(s^{-1})	3.4±0.1	1.2±0.1	3.4±0.1	2.6±0.1	13.9±0.1[b]	4.2±0.1[b]
$K_{M(\mathrm{RuBP})}(\mu\mathrm{M})$	18.8±3.2	92±9	56±6	44±2	54±3[b]	3.9±1[b]
$K_{M(\mathrm{CO_2})}(\mu\mathrm{M})$	10.7±0.6	3.3±0.4	27.9±0.4	9.3±0.8	284±30[c,†]	67±10[e,†]
$K_{M(\mathrm{O_2})}(\mu\mathrm{M})$	295±71	374±92	467±22	890±440*	529±50[d,†]	170±20[f,†]
Ω	82±2	166±6	113±1	167±3	43±1[c]	12±2[g,†]
Calculated model parameters						
$k_{cat}(s^{-1})$	3.3...3.5	1.1...1.3	3.3...3.5	2.5...2.7	13.8...14.0	4.1...4.3
$k_{oxy}(s^{-1})$	0.77...1.60	0.49...1.30	0.45...0.56	0.66...2.57	0.48...0.76	0.57...1.43
$k^+_{ER}(\mu M^{-1}s^{-1})$	0.15...0.22	0.011...0.016	0.053...0.070	0.054...0.064	0.24...0.27	0.84...1.48
$\gamma(\mu M^{-1})$	0.088...0.099	0.27...0.35	0.035...0.036	0.099...0.118	0.0032...0.0039	0.013...0.018
$\omega(\mu M^{-1})$	0.0027...0.0045	0.0021...0.0036	0.0020...0.0022	0.0007...0.0022	0.0017...0.0029	0.0053...0.0067

Data from [a][29], [b][11], [c][30], [d][31], [e][32], [f][33], [g][34].

*The $K_{M(\mathrm{O_2})}$-value has been estimated from the measured $K^{\mathrm{air}}_{M(\mathrm{CO_2})}$ value obtained at athmospheric oxygen levels (see Supporting Text S2).

†No experimental error given in the original publication. The error was estimated to be approximately 10%.

Table 2: Parameters for wild-type tobacco for the simple model

parameter	value	parameter	value
k^+_{ER}	0.15 $(\mu\mathrm{Ms})^{-1}$	k^-_{ER}	0.048 s^{-1}
k^+_{ERC}	0.302 $(\mu\mathrm{Ms})^{-1}$	k^-_{ERC}	0.02 s^{-1}
k^+_{ERO}	0.0012 $(\mu\mathrm{Ms})^{-1}$	k^-_{ERO}	0.02 s^{-1}
k^+_{EI1}	0.0152 s^{-1}	k^-_{EI1}	0.0017 s^{-1}
k^+_{EI2}	0.1 s^{-1}	k^-_{EI2}	0 s^{-1}
k^+_X	0 s^{-1}	k^-_X	0 s^{-1}
k^+_P	0 s^{-1}	k^-_P	$5.5{\cdot}10^{-4}$ s^{-1}
k_{cat}	3 s^{-1}	k_{oxy}	1.125 s^{-1}

Figure Captions

Figure 1: Schematic representation of the model describing the enzyme kinetics of RuBisCO. Bold arrows represent the fast reactions of catalysis, which comprise the main carboxylation and oxygenation pathways. Side reactions are denoted by the thin arrows, leading to the formation of enzyme-inhibitor complexes highlighted in dark blue.

Figure 2: Effect of the fast rate constants on various observed quantities. Red fields denote sensitivities near $+1$, blue fields near -1 and white fields denote a response coefficient of or near 0.

Figure 3: Influence of the rates of inhibitor formation and backward transformation on the fallover extent and characteristic time under anaerobic (A) and aerobic conditions (B). The solid lines depict the relative change of the fallover extent as functions of the relative change of the rate constant of inhibitor formation (blue) and for the reactivation (red) of the active site. In the anaerobic case (A), reactivation is achieved by back transformation, in the aerobic case (B) by inhibitor release. The dashed lines indicate the corresponding relative changes of the observed fallover rate constant k_{obs}. Insets depict the simulated time courses of fallover for the original parameter set (see Table 2). In the insets, initial and final rates, as well as the half-time, are indicated. External concentrations were set to 500 μM RuBP, 0 μM XuBP, 0 μM PDBP, 250 μM CO_2 and oxygen was 0 μM for the anaerobic case (A) and 250 μM for the aerobic case (B). Total enzyme concentration was normalized to unity.

Figure 4: The effect of carbon dioxide and oxygen concentrations on the fallover extent. A) Fallover extent is plotted as a function of both substrate concentrations. B) For selected conditions the fallover extent is plotted as a function of a single substrate concentration. In the upper panel, oxygen is fixed at atmospheric level and the CO_2 concentration is given in equivalents of applied $NaHCO_3$. In the lower panel, CO_2 was fixed at an equivalent of 10 mM $NaHCO_3$ and oxygen level is given in percents of the ambient gas. The values were calculated with model parameters given in Table 2. The concentration of RuBP was set to 500 μM, the inhibitors XuBP and PDBP were set to zero.

Figure 5: The effect of external carbon dioxide and oxygen concentrations on the fallover rate. A) Fallover half time is plotted as a function of both substrate concentrations. B) The two eigenvalues of the reduced system matrix are given together with the apparent fallover rate k_{obs} determined as a fit of one exponential to the weighted sum of the two exponentials. The values were calculated with model parameters given in Table 2. The concentration of RuBP was set to 500 μM, the inhibitors XuBP and PDBP were set to zero.

Figure 6: Model extension. Panel (A) recapitulates the simple model depicted in Fig. 1. The new model (B) dissects and extends binding steps that are highlighted in the blue box in (A). The binding of the pentose phosphates are described as two steps. First, substrates (RuBP and XuBP) are bound to form the enzyme-substrate complexes ER and EI1, respectively. In a second step, the enolization results in the enediol intermediates bound to the enzyme (complexes EE1 and EE2) which represent the same intermediate but differ in the local environment within the active center. From these, a third inhibitor, associated with DP1P, can be formed. Bold arrows designate the fast reactions in catalysis, enzyme-inhibitor complexes are shown in dark blue.

Figure 7: The biphasic inhibitory effect of XuBP as predicted by the model. The effect of incubation time on the initial catalytic rate is plotted for various inhibitor concentrations. Simulations were performed with parameters resembling wild-type tobacco RuBisCO (see Supplementary Table S1). During incubation, the external concentration of RuBP was set to zero, thereafter fixed to 500μM. Simulation was carried out for aerobic conditions (250 μM CO_2, 250 μM oxygen, 0 μM PDBP).

Figure 8: Two different configurations of RuBisCO with enediol intermediate. The arrows indicate the hydrogen movement responsible for creating the shown situation. In case of RuBP (A) the removed hydrogen is bound to the carboxylated lysine residue (KCX). For XuBP (B) the hydrogen has to be accepted by some other nucleophilic group, possibly the water molecule opposite to the KCX group.

Figure 9: Simulated carboxylation of XuBP for wildtype RuBisCO. Shown are the time courses (A) of the catalytic rate (bold line) and relevant intermediary enzyme-substrate complexes (dashed lines). The parameters are given in Supplementary Table S1. The external concentration of XuBP was fixed to 50μM, RuBP concentration was considered a variable with initial value 0, CO_2 and oxygen were fixed at 250 μM, PDBP was set to zero. In (B), response coefficients for the most important parameters influencing characteristic properties of the dynamics are given.

Figure 10: Closed RuBisCO active site. The atoms of RuBP are colored depending on their type. Other structures are single-colored: Blue, large subunit A (surface); gray, large subunit B (lines); green, Mg^{2+} ion; violet, Lys-334 of subunit A; orange, Leu-335 of subunit A; yellow, Phe-127 of subunit B. The three depicted amino acids are shielding the substrate from the solvent. With a less flexible amino acid in the position of Leu-335, such as Val, closure in the same manner requires backbone shifting and/or is less efficient. Exemplary RuBisCO from *Chlamydomonas reinhardtii* (PDB entry 1GK8 [48]) shown, full hexadecamer geometry kindly provided by Prof. Andersson (Uppsala).

Figure 11: Simulated carboxylation of XuBP for the Val-335 mutant. Shown are the time courses (A) of the catalytic rate (bold red line), concentration of free RuBP (dashed blue line) and the rate of the reversed enolization (-v_{EE1}, thin black line). Parameters are given in Supplementary Table S1 (right column). External conditions are as for Fig. 9. In (B), response coefficients for the most influential parameters on the characteristic properties of the dynamics are given.

Figure 1

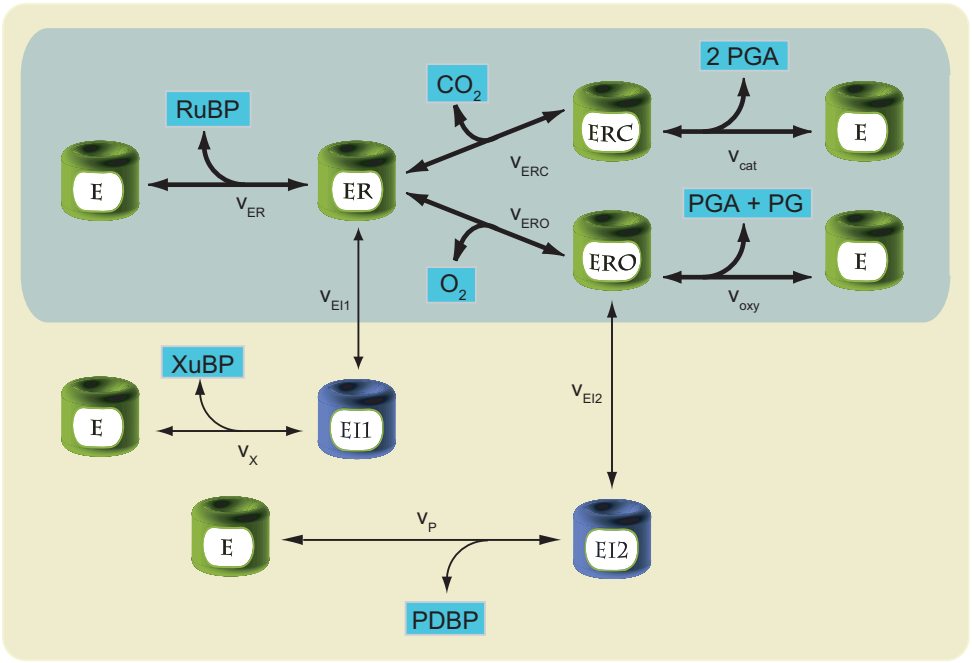
RuBP
CO2
2 PGA
E
ER
ERC
E
VER
VERC
Vcat
VERO
PGA + PG
O2
ERO
E
VEI1
Voxy
XuBP
VEI2
E
EI1
VX
E
VP
EI2
PDBP

Figure 2

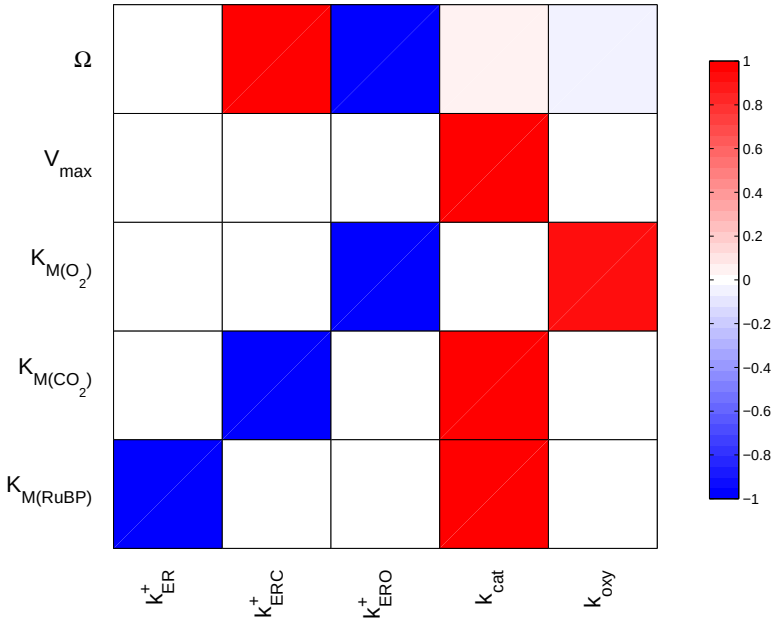
Ω
V max
K M(O2)
K M(CO2)
K M(RuBP)
k+ ER
k+ ERC
k+ ERO
k cat
k oxy
1
0.8
0.6
0.4
0.2
0
−0.2
−0.4
−0.6
−0.8
−1

Figure 3

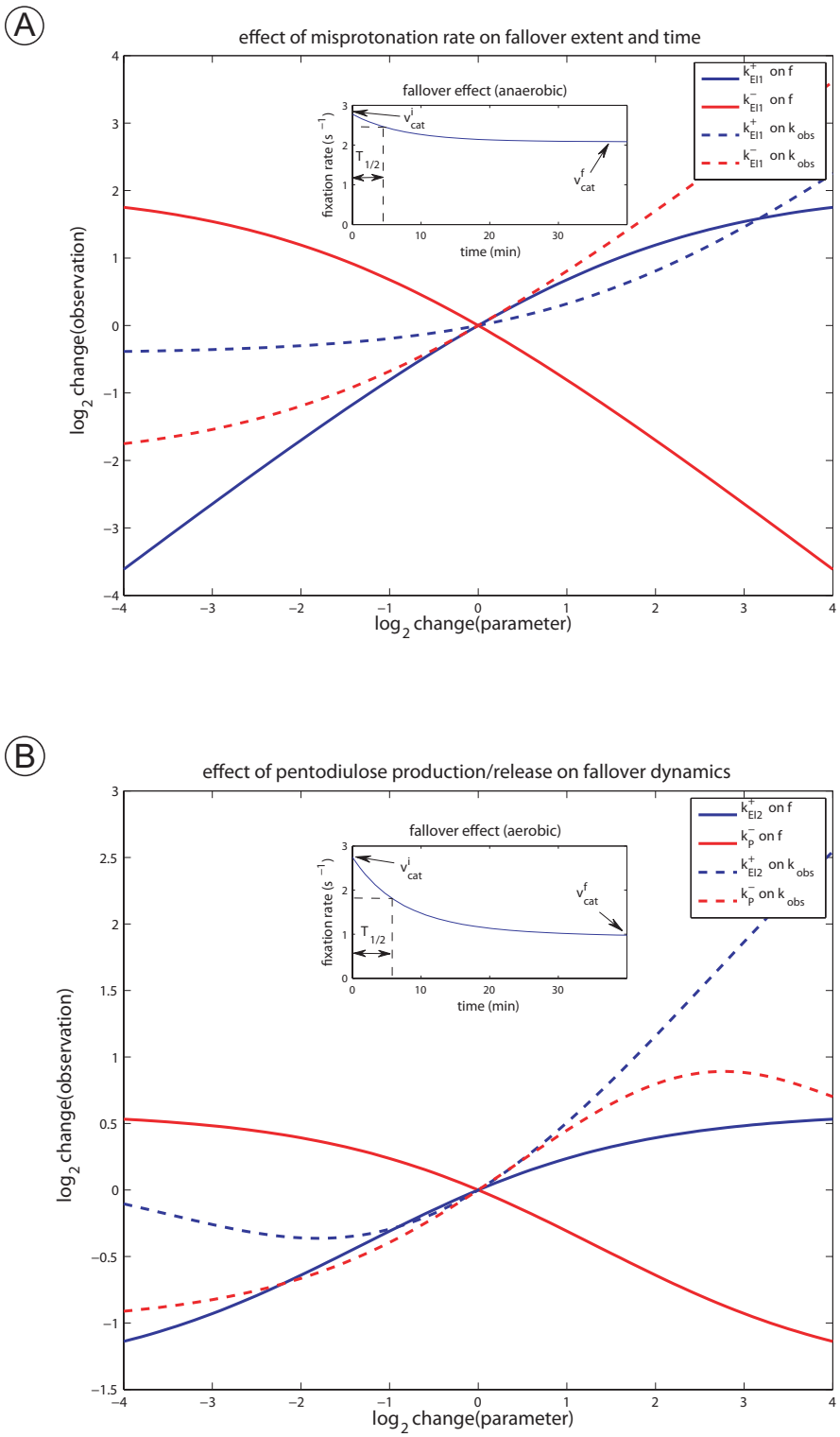
A
effect of misprotonation rate on fallover extent and time
fallover effect (anaerobic)
fixation rate (s^{-1})
time (min)
v^i_{cat}
v^f_{cat}
$T_{1/2}$
k^+_{EI1} on f
k^-_{EI1} on f
k^+_{EI1} on k_{obs}
k^-_{EI1} on k_{obs}
log$_2$ change(observation)
log$_2$ change(parameter)
B
effect of pentodiulose production/release on fallover dynamics
fallover effect (aerobic)
fixation rate (s^{-1})
time (min)
v^i_{cat}
v^f_{cat}
$T_{1/2}$
k^+_{EI2} on f
k^-_P on f
k^+_{EI2} on k_{obs}
k^-_P on k_{obs}
log$_2$ change(observation)
log$_2$ change(parameter)

Figure 4

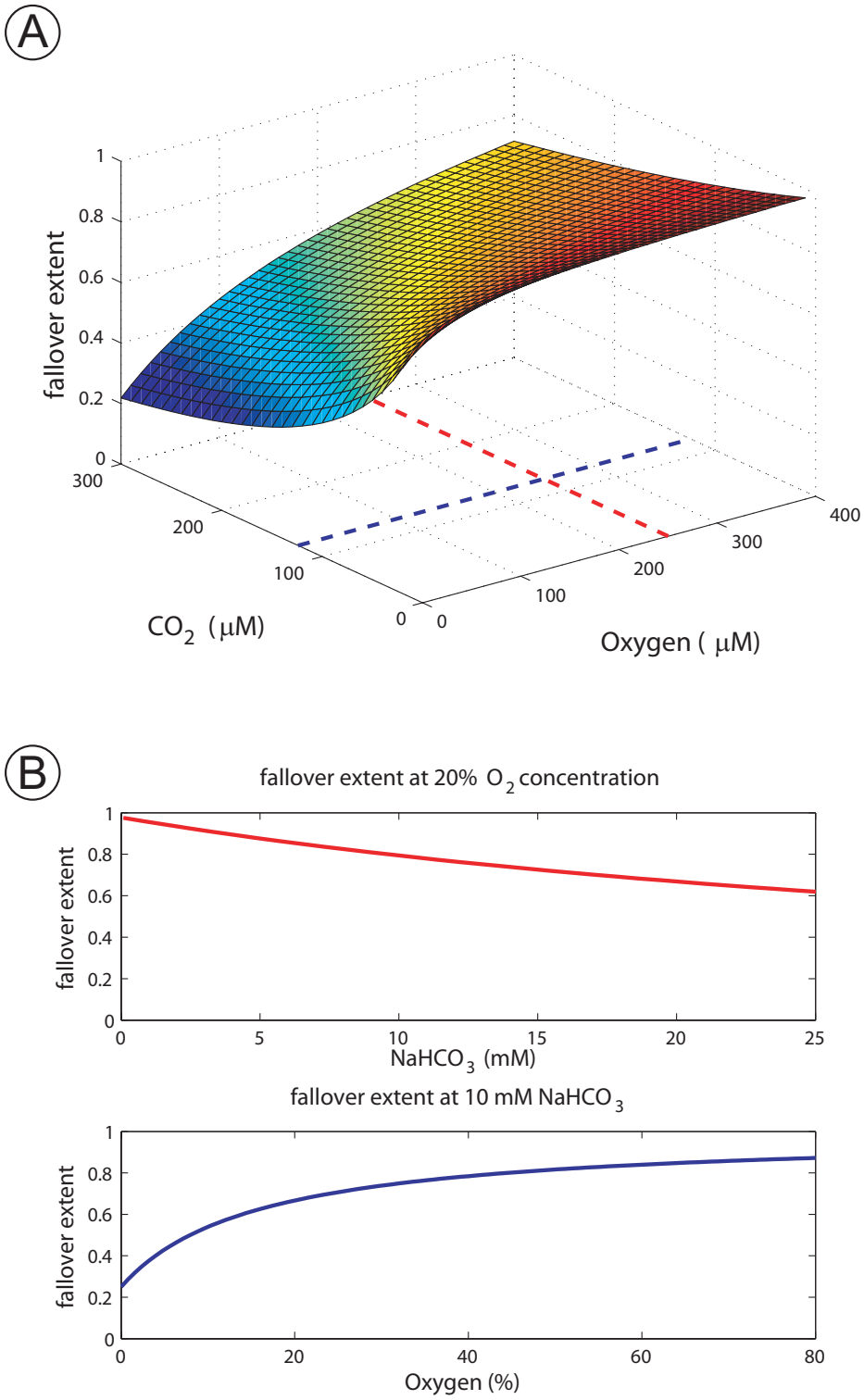
A
fallover extent
1
0.8
0.6
0.4
0.2
0
300
200
100
0
CO2 (μM)
0
100
200
300
400
Oxygen (μM)
B
fallover extent at 20% O2 concentration
fallover extent
0
0.2
0.4
0.6
0.8
1
0
5
10
15
20
25
NaHCO3 (mM)
fallover extent at 10 mM NaHCO3
fallover extent
0
0.2
0.4
0.6
0.8
1
0
20
40
60
80
Oxygen (%)

Figure 5

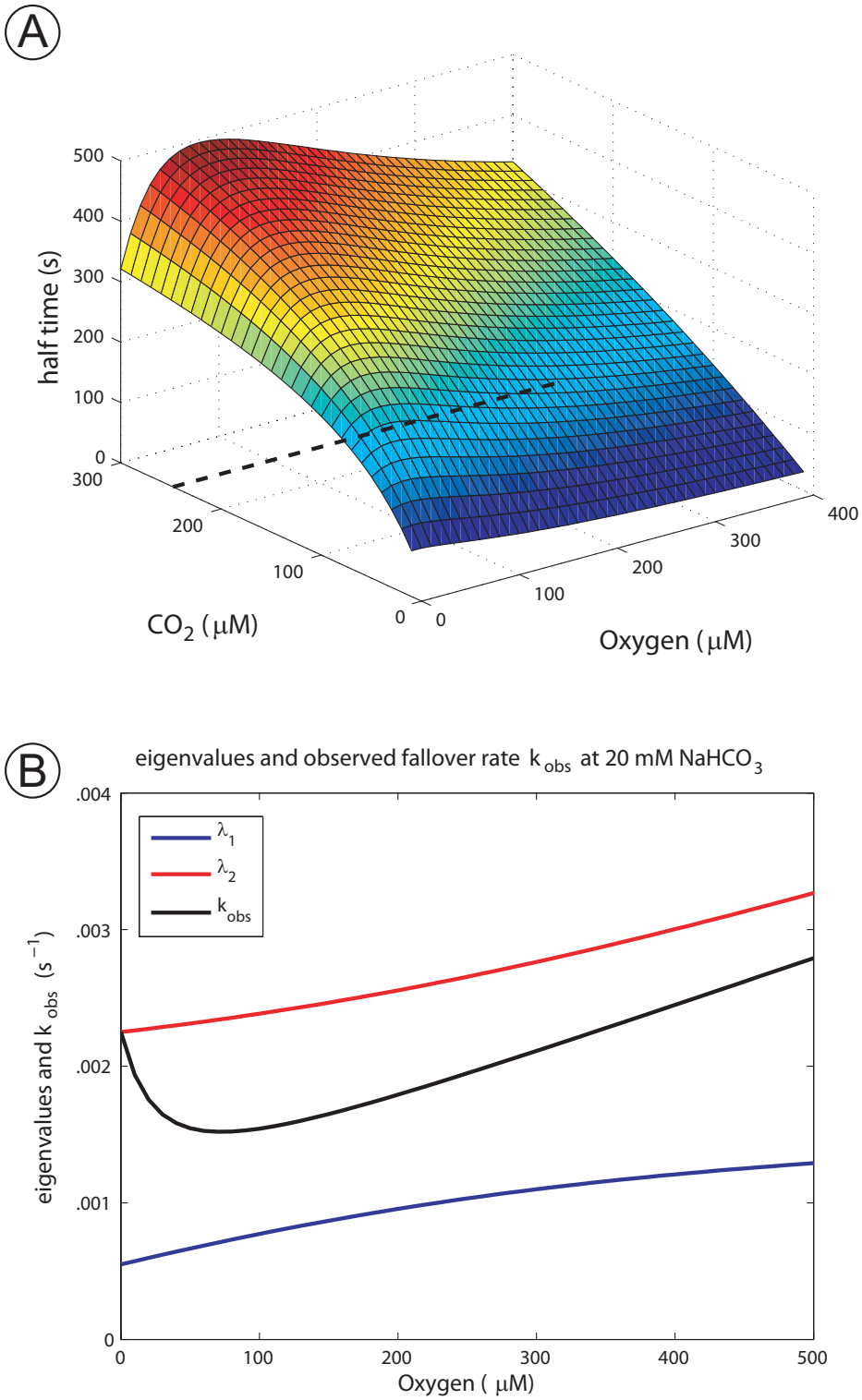
A
half time (s)
500
400
300
200
100
0
300
200
100
0
CO2 (μM)
0
100
200
300
400
Oxygen (μM)
B
eigenvalues and observed fallover rate k obs at 20 mM NaHCO3
λ1
λ2
k obs
eigenvalues and k obs (s−1)
.004
.003
.002
.001
0
0
100
200
300
400
500
Oxygen (μM)

Figure 6

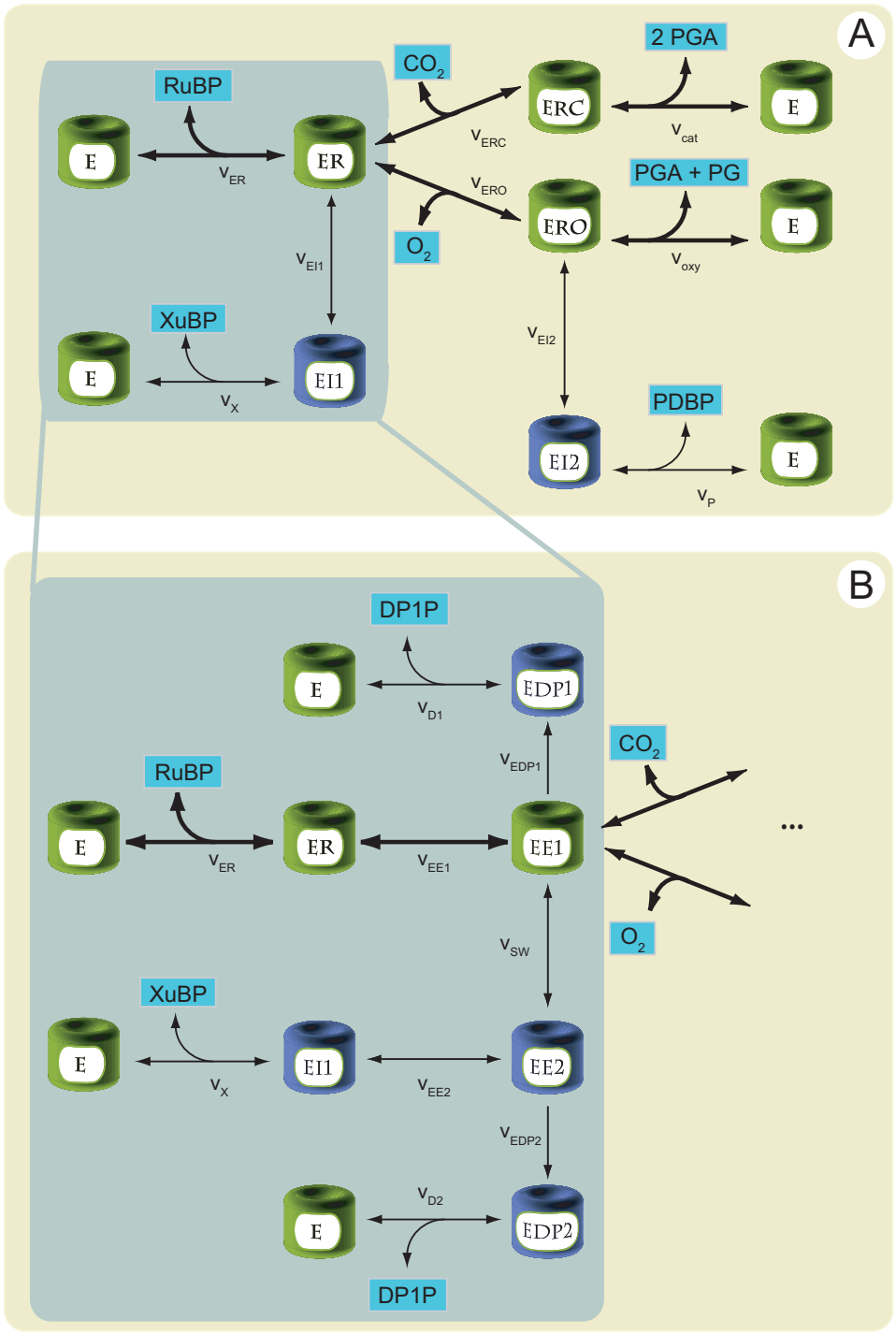
A
RuBP
CO2
2 PGA
E
ER
ERC
E
VER
VERC
Vcat
VERO
PGA + PG
ERO
E
O2
Voxy
VEI1
VEI2
XuBP
E
EI1
VX
PDBP
EI2
E
VP
B
DP1P
E
EDP1
VD1
VEDP1
CO2
RuBP
E
ER
EE1
...
VER
VEE1
VSW
O2
XuBP
E
EI1
EE2
VX
VEE2
VEDP2
VD2
E
EDP2
DP1P

Figure 7

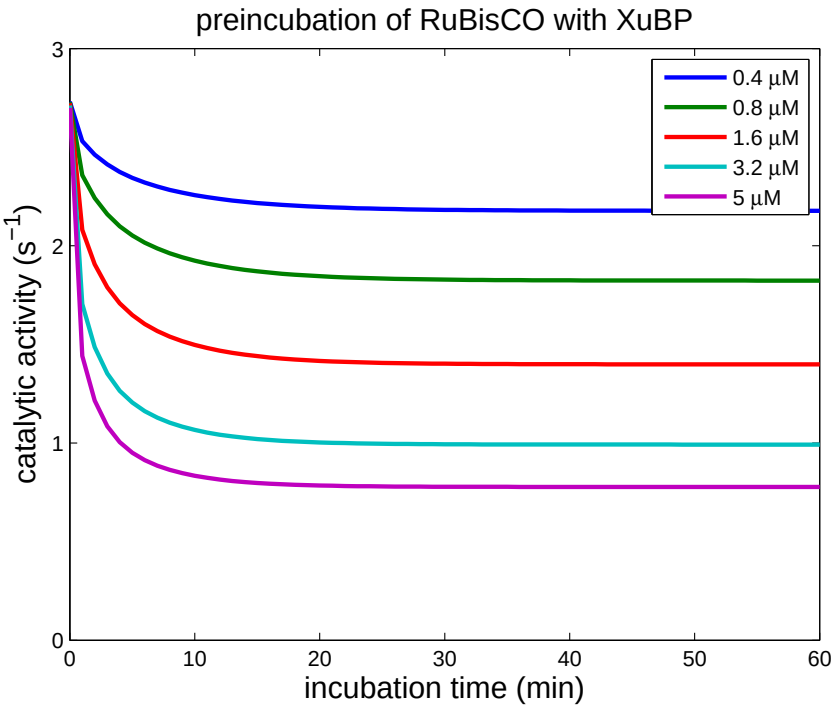
preincubation of RuBisCO with XuBP
0.4 µM
0.8 µM
1.6 µM
3.2 µM
5 µM
catalytic activity (s^{-1})
incubation time (min)
0
1
2
3
0
10
20
30
40
50
60

Figure 8

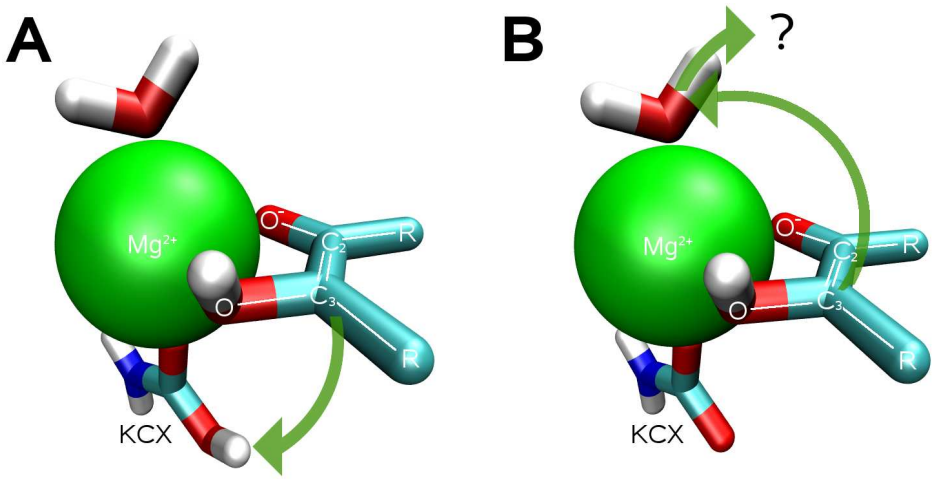

Figure 9

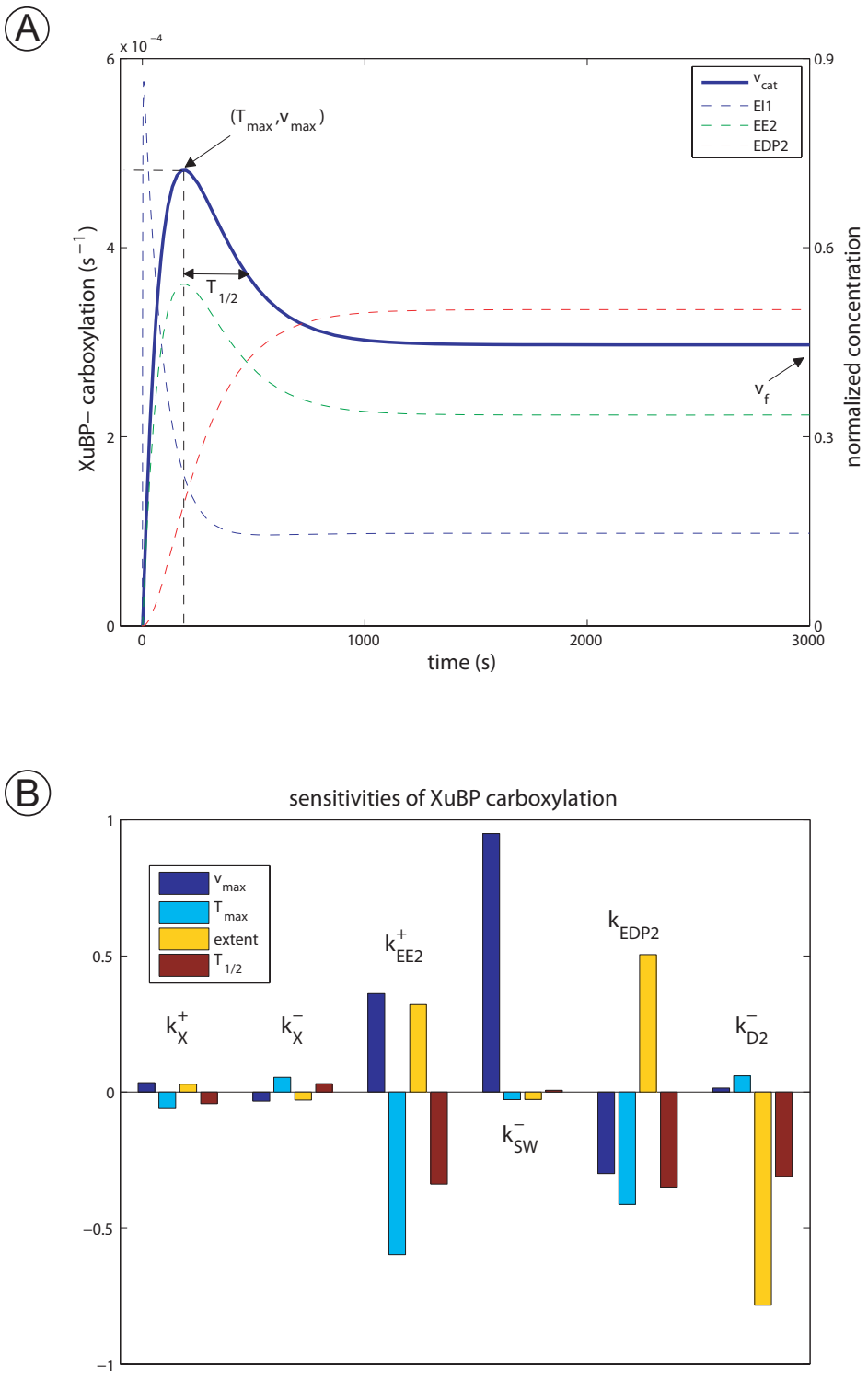
A
x 10^-4
6
4
2
0
0.9
0.6
0.3
0
0
1000
2000
3000
time (s)
XuBP− carboxylation (s^-1)
normalized concentration
v_cat
EI1
EE2
EDP2
(T_max, v_max)
T_1/2
v_f
B
sensitivities of XuBP carboxylation
1
0.5
0
−0.5
−1
v_max
T_max
extent
T_1/2
k_X^+
k_X^−
k_EE2^+
k_SW^−
k_EDP2
k_D2^−

Figure 10

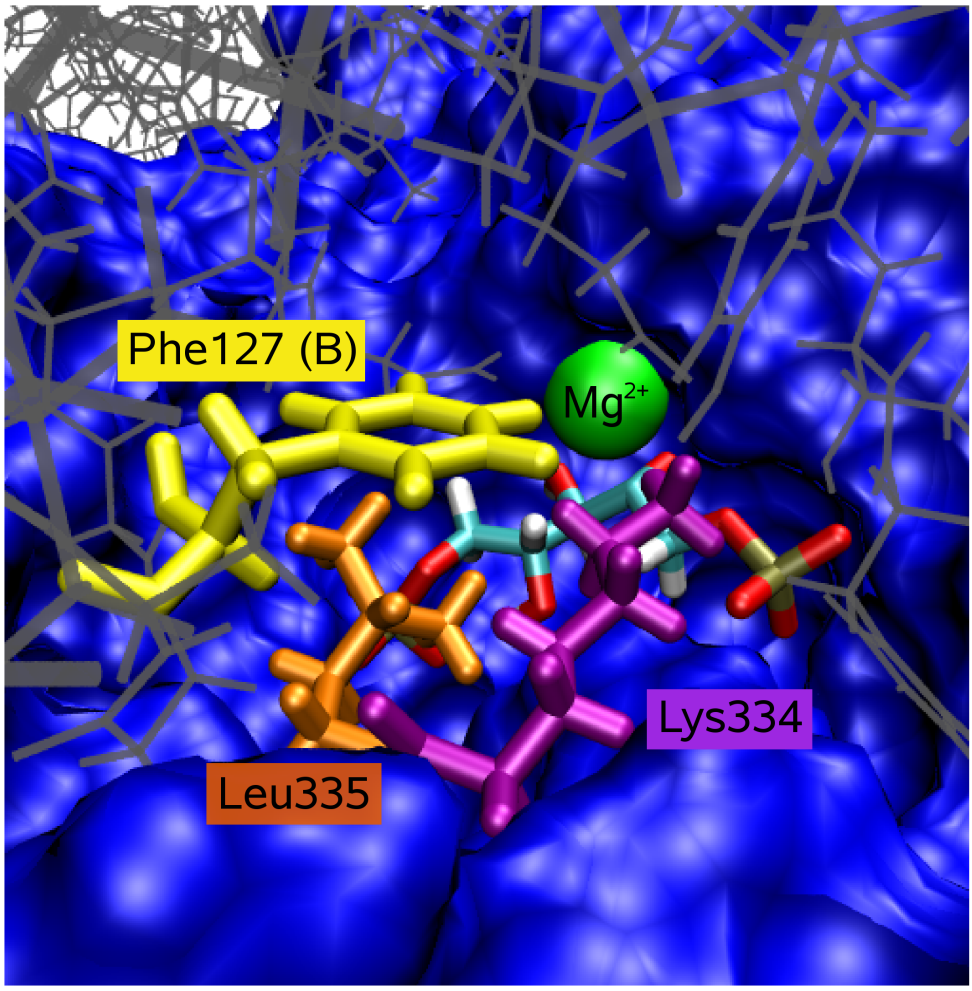

Figure 11

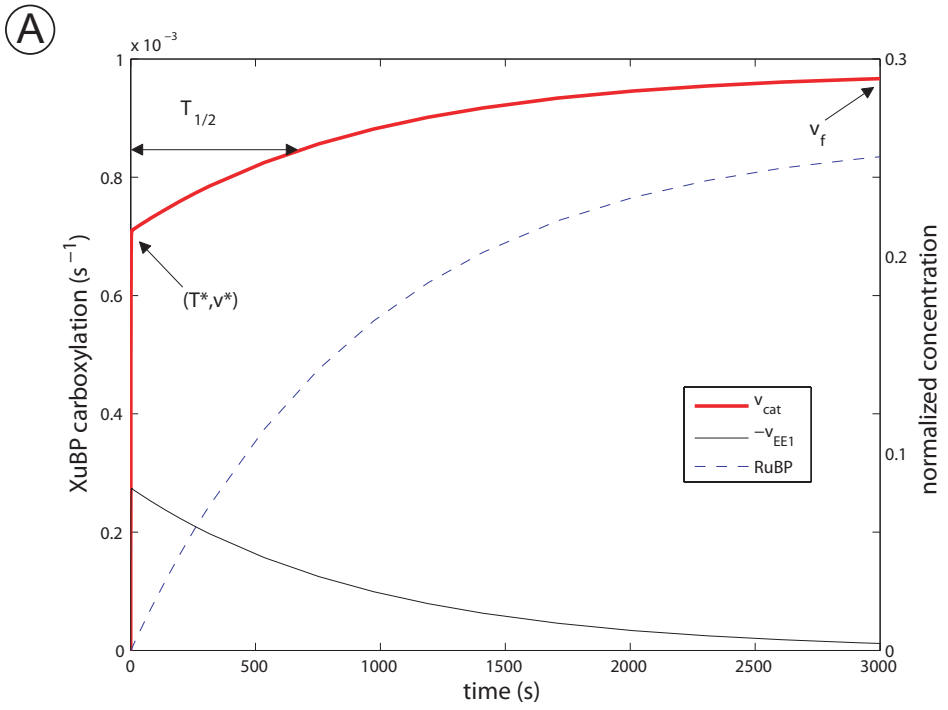
A
x 10^−3
T1/2
vf
(T*,v*)
XuBP carboxylation (s^−1)
normalized concentration
time (s)
vcat
−vEE1
RuBP

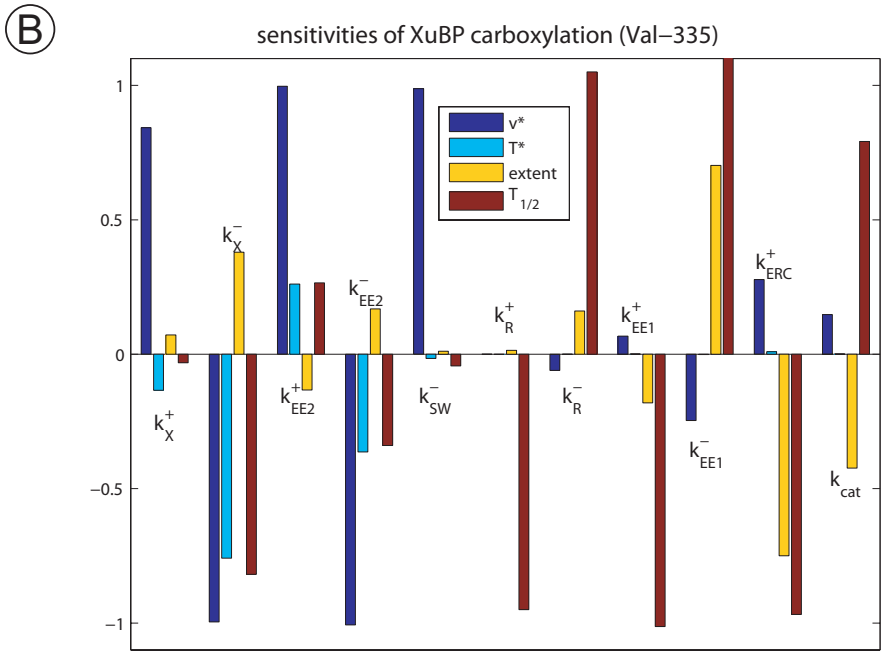
B
sensitivities of XuBP carboxylation (Val−335)
v*
T*
extent
T1/2
k+X
k−X
k+EE2
k−EE2
k−SW
k+R
k−R
k+EE1
k−EE1
k+ERC
kcat